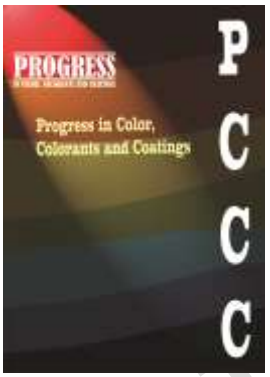
ACCEPTED MANUSCRIPT

Accepted Manuscript



Title: Multi criteria optimization of Self curable CNSL based Epoxy Coatings using Entropy, CRITIC-Weighted TOPSIS and Grey Relational Analysis

Authors: Dev Tiwari, Radha Sachan, Arun Maithani, Durgesh Kumar Soni

Manuscript number**: PCCC-2608-1532**

To appear in: Progresss in Color, Colorants and Coatings

Received: 18 August 2026

Final Revised: 23 October 2026

Accepted: 25 October 2026

Please cite this article as:

D. Tiwari, R. Sachan, Ar. Maithani, D. Kumar Soni, Multi criteria optimization of Self curable CNSL based Epoxy Coatings using Entropy, CRITIC-Weighted TOPSIS and Grey Relational Analysis Prog. Color, Colorants, Coat., 20 (2027) XX-XXX.

DOI: 10.30509/pccc.2026.167861.1532

This is a PDF file of the unedited manuscript that has been accepted for publication. The manuscript will undergo copyediting, typesetting, and review of the resulting proof before it is published in its final form

ACCEPTED MANUSCRIPT

Multi Criteria)ptimization of Self Curable CNSL Based Epoxy Coatings Using Entropy, CRITIC-Weighted TOPSIS and Grey Relational Analysis

D. Tiwari, R. Sachan, A. Maithani, D. Kumar Soni *

Department of Paint Technology, School of Chemical Technology, Harcourt Butler Technical University, Kanpur-208002

Corresponding author email address: durgesh.soni@hbtu.ac.in

Accepted Manuscript

Abstract:

Five self-curable epoxidized phenol-modified cardanol novolac (EPMCN-1 to EPMCN-5) coatings, varying in phenol content (0%-40%, molar basis), were prepared. FTIR, ^{1}H NMR, DSC, and TGA confirmed novolac formation, epoxidation, and the self-cure mechanism of the synthesized resins. Mechanical properties (pencil hardness, scratch hardness, cross-cut adhesion, impact resistance) and solvent resistance (acetone, xylene, MEK) were evaluated. Chemical resistance to acid, alkali, and water was assessed by monitoring gloss retention and adhesion. Acid and water exposure produced negligible changes across all formulations, but alkali exposure caused pronounced, formulation-dependent gloss loss, well described by a first-order empirical model ($R^2 \geq 0.975$). Rate constants showed a roughly 2.35-fold difference in alkali durability associated with phenol content. To rank the formulations, entropy and CRITIC weighting were combined with grey relational analysis (GRA) and TOPSIS. All four method-weighting combinations, applied to the dataset, produced the order: EPMCN-4 > EPMCN-3 > EPMCN-2 > EPMCN-5 > EPMCN-1, also seen in solvent resistance. Alkali gloss retention showed the largest relative variation among the criteria measured (entropy

ACCEPTED MANUSCRIPT

weight 0.358, CRITIC weight 0.105), reflecting its importance in the dataset. These results identify EPMCN-4 as the best-balanced formulation, demonstrating that time-resolved degradation kinetics combined with multi-criteria decision analysis gives a more defensible ranking than single-endpoint comparison.

Keywords: Alkali Degradation; Bio-based Epoxy; Chemical Resistance; Gloss Retention; Solvent Resistance; Structure-Property Relationship.

1. Introduction

Epoxy resins are among the most important resins for protective coating systems. They provide good adhesion, chemical resistance, and mechanical strength. However, most commercial epoxy resins are still made from bisphenol A (BPA). BPA is petroleum-derived and a known endocrine disruptor. It exhibits toxic, estrogenic, mutagenic, and carcinogenic effects, and its use is increasingly restricted [1]. There is now a strong push to replace them with renewable, bio-based materials [2]. Bio-based resins lower the carbon footprint of coatings and reduce dependence on fossil resources. These concerns have driven the search for safe, bio-based epoxy resins.

Cashew nut shell liquid (CNSL), a low-cost, non-edible by-product of the cashew industry, is a promising renewable feedstock that does not compete with the food supply, and has been used for a long time in paints and coatings [3, 4]. Its main component, cardanol, is a phenol bearing a C_{15} unsaturated side chain with three reactive sites: the phenolic hydroxyl, the aromatic ring, and the side-chain double bonds [4, 5], enabling a wide range of chemical modifications; the long aliphatic chain also acts as an internal

ACCEPTED MANUSCRIPT

plasticizer and imparts hydrophobicity to the resulting polymer. Performance can be raised further by reacting cardanol with formaldehyde, which yields a higher-functionality novolac, and epoxidizing it, further enhancing, the thermal and mechanical properties [6, 7]. Such cardanol-based epoxidized novolac resins have been studied for coatings [8, 9] and are often toughened by blending with reactive rubbers such as carboxyl-terminated butadiene-acrylonitrile copolymer [10, 11], which rely on extern-al amine or anhydride hardeners. Cardanol novolacs have indeed been used as a curing agent for conventional epoxy resins [12]. The novolac's phenolic hydroxyl groups react directly with oxirane rings, making the resin self-curable. Since phenol content sets the hydroxyl-to-oxirane ratio, it governs crosslink density and film properties.

Multi-criteria decision-making (MCDM) is a systematic decision-analysis approach used to evaluate and rank a set of alternatives when several, often conflicting, criteria must be considered simultaneously. Instead of selecting an alternative on the basis of a single response, MCDM integrates the performance of all relevant criteria into a common decision framework so that an overall and balanced assessment can be made [11, 12]. This approach is particularly relevant to coating formulation, because coating performance is inherently multidimensional. A formulation is expected to provide an appropriate combination of hardness, flexibility, adhesion, impact resistance, gloss, and chemical resistance, yet improvement in one property does not necessarily result in improvement in the others [13-16]. For instance, an increase in hardness may be accompanied by reduced flexibility or impact resistance, while superior chemical resistance may not correspond to the highest gloss or adhesion. In addition, these properties are measured using different scales, units, and response directions, which

Accepted Manuscript

ACCEPTED MANUSCRIPT

makes direct comparison difficult. Therefore, selection of the optimum formulation cannot be reliably based on a single property or on simple side-by-side comparison of experimental results.

In polymer composites, Grey Relational Analysis is often paired with the Taguchi method to optimize several properties together. It has been applied to the wear behavior of metal–ceramic composites [17] and to the tensile and flexural properties of natural-fiber polymer composites [18]. In coatings, TOPSIS with entropy weights has been used to rank coating materials [19], and an AHP–TOPSIS method has been used to choose a coating for magnesium alloys [20]. In each case, the method turns a large, multi-property dataset into a clear ranking.

Studies on CNSL/cardanol-derived epoxy coatings focused on the synthesis of cardanol epoxies, modification with external epoxy components, development of cardanol-derived curing agents, or evaluation of selected mechanical, thermal and corrosion-resistance properties [21-24]. Self-curable cardanol epoxies have also been reported but are completely synthesized from monomeric cardanol [25]. Cardanol novolacs investigated previously were principally employed as curing agents or modifiers for conventional epoxy matrices [10, 26]. Similarly, although multi-criteria decision-making methods such as TOPSIS and Grey Relational Analysis have been applied in coating science, their use was largely centred on raw material selection, coating-colour formulation, and optimization of deposition or surface-treatment parameters [27, 28]. The present work addresses these two research gaps by establishing phenol content as a variable within a series of self-curable epoxidized phenol-modified cardanol novolac (EPMCN) coatings and quantitatively linking this compositional variation to the resulting multi-property

ACCEPTED MANUSCRIPT

coating response. Rather than identifying an optimum formulation from a single performance parameter. Mutually competing properties like flexibility, hardness, adhesion, impact resistance, gloss and chemical resistance are considered simultaneously. In addition, the time-dependent response of the coatings during alkaline exposure was evaluated using an empirical first-order model fitted to the experimental observations.

A further methodological contribution is the use of two independent, data-driven weighting approaches-Entropy and CRITIC-together with TOPSIS and Grey Relational Analysis. Entropy weighting reflects the discriminatory information contained in the experimental responses, whereas CRITIC additionally accounts for both criterion contrast and inter-criterion correlation. Using more than one ranking method improved the reliability of formulation selection. The agreement among the different MCDM approaches supports the robustness of the final ranking and strengthens the novelty of the proposed evaluation framework. The study consequently advances cardanol-based coating research from property-by-property characterization toward quantitative, performance-balanced formulation design.

Accepted Manuscript

2. Experimental

2.1 Materials

Single distilled Cardanol was obtained from Kumar Rotoflex Pvt Ltd, Kanpur. Formaldehyde (37% solution) which was used for formylation, Oxalic Acid which was used as a catalyst, Methanol, which was used to dissolve the catalyst, Hydrogen Peroxide (H_2O_2) and Formic Acid which werfore used to prepare in-situ performic acid for epoxidation, Chlorobenzene, Potassium Acid Phthalate, Hydrobromic Acid and Acetic

ACCEPTED MANUSCRIPT

Acid, which were used for the determination of epoxy equivalent weight were procured from M/s Molychem India LLP, Mumbai. Pyridine was procured from SRL Pvt. Ltd and Acetic Anhydride from SD Fine-Chem Ltd.

2.2 Synthesis of Phenol Modified Cardanol Novolac (PMCN) and Epoxidised Phenol Modified Cardanol Novolac (EPMCN)

(a) Synthesis of PMCN: Novolac resins were synthesized with 0% to 40% phenol on a molar basis. Novolac resins were synthesized with phenol-to-formaldehyde ratio of 1:0.8 (here phenol means cardanol/cardanol + phenol). Oxalic Acid (2% by weight based on cardanol/cardanol + phenol) was used to catalyze the reaction. Cardanol was charged in a 3-neck flask. It was heated to 110°C. Formaldehyde (37%) and phenol were charged into the flask at a controlled rate with the help of a burette for 4 hours. After the addition was complete, the reaction mixture was maintained at the same temperature for another 2 hours.

(b) Synthesis of EPMCN: The synthesized PMCNs were taken in a 3 neck flask and the calculated amount of formic acid was charged in the flask along with the PMCN. H_2O_2 was charged through a burette over a time period of 3-4 hours. The amount of PMCN, formic acid and H_2O_2 was based on the ratio which is unsaturation: formic acid: H_2O_2 = 1:1: 2.8. During the addition of H_2O_2 the temperature was kept at 5-10 °C. After the addition of H_2O_2, the temperature was slowly raised to 40 -45 °C. The resin was reduced to 70-75 % solids with ethyl acetate as solvent. After completion, the reaction mixture was neutralized thoroughly with sodium bicarbonate solution 3-4 times and then the

ACCEPTED MANUSCRIPT

reaction mixture was washed with hot water. Then the organic layer was obtained and anhydrous sodium sulphate was added to remove the traces of water present in the organic layer.

2.3 Surface Preparation and Preparation of Samples:

Panels of dimension 100 × 150 mm made of mild steel (MS) and Tin were used as test panels for characterisation and evaluation of the coatings. The surface of the panels was cleaned using emery cloth of grit size 200 and 400. Then the panels were wiped with xylene and IPA one after the other with a clean white cotton cloth.

Then the coatings were applied to the panels with a 100 µm bar applicator by adjusting the solid content of the coating to 50-60% (on a solid basis). 1% by wt. of 2-Methylimidazole was used [29]. 2-methylimidazole was employed as a curing accelerator as it catalyzes epoxide ring-opening via nucleophilic attack of its tertiary ring nitrogen without actually being consumed in the curing reaction. The coated panels were kept at room temperature for approximately 2 hours to allow initial solvent flash-off before baking and then heated to 120 °C for 20 minutes as DSC showed T_{onset} as low as 117 °C for some formulations in the series [30]. Then the temperature was raised to 140 °C for 15 minutes for removal of residual butyl cellosolve and lastly raised to 190°C for 30 minutes to drive the system toward a higher degree of cure [25, 30]. Then the panels were kept at room temperature for 24 hours and then other testing was performed.

2.4. Characterisation of coatings and testing of film properties:

The films produced by the curing of the resin with different curing agents were analysed as follows:

ACCEPTED MANUSCRIPT

a) Impact resistance was conducted using a Tubular Impact Tester of Sheen, UK, following ASTM D-2794.

b) Scratch hardness testing was conducted using an automatic scratch hardness tester (Sheen, UK) according to ASTM D-7027.

c) Pencil hardness was determined using Mitsubishi Uni pencils (Mitsubishi Pencil Co., Ltd., Japan) in accordance with ASTM D3363.

d) Adhesion of the films was assessed using a Cross Hatch Adhesion Tester of Caltech, India according to ASTM D-3359.

e) Flexibility of the films was tested using a Conical Mandrel from Khushboo Scientific according to ASTM D-522.

f) Resistance to water, acid and alkali was assessed according to ISO-2812-1-2017 where coated panels were immersed in the test medium (5% HCl for acid resistance, 5% NaOH for alkali resistance, distilled water for water resistance) for 36 h at 25°C, with 60° gloss measured before and after immersion, and additionally at 6 h intervals over the 36 h period for alkali exposure. All tests were performed in triplicate.

g) Gloss of the coatings was evaluated through Shenzhen 3nH Technology Co. Ltd, China according to ASTM D-523.

h) Dry film thickness of the coatings was measured through DFT Meter of Elcomter Ltd U.K. according to ASTM D-7091.

i) Solvent resistance was assessed by the solvent rub method according to ASTM D5402 with xylene, acetone and MEK and dry film thickness was measured

ACCEPTED MANUSCRIPT

before and after rubbing to determine percentage thickness loss. The test was performed in triplicate.

j) *Fourier Transform Infrared spectroscopy:* Fourier-transform infrared (FTIR) spectra of cardanol, phenol-modified cardanol novolac (PMCN), epoxidized phenol-modified cardanol novolac (EPMCN) and the cured films of EPMCNs were recorded using an FTIR spectrometer (PerkinElmer, USA) over the mid-infrared range of 4000–400 cm^{-1}. All spectra were obtained from neat samples on a 100% solids basis.

k) H^1NMR spectroscopy: H^1NMR spectra for the samples was recorded at room temperature on a $_1H^1$ NMR spectrophotometer (JNM ECZ-500MHz JEOL, Ltd) working at 500MHz using deuterated chloroform ($CDCl_3$) as solvent.

l) Thermogravimetric analysis: The thermogravimetric analysis of the samples was performed on a 100% solids basis using SDT-650 (TA instrument, USA). The temperature range for analysis was 30°C to 800°C at a rate of 10 °C/min.

m) Differential Scanning Colorimetry: Differential scanning calorimetry (DSC) was performed on a Mettler Toledo simultaneous thermogravimetric–differential scanning calorimetry analyzer over a temperature range of 37-250 °C, at a heating rate of 5 °C/min under a nitrogen atmosphere. Liquid resins and cured films of 3mg were placed in aluminium pans, with an empty pan of the same type used as a reference.

2.5. Multi-criteria evaluation of coating performance

The five coatings were assessed against nine film-performance criteria (flexibility, pencil

ACCEPTED MANUSCRIPT

hardness, scratch hardness, cross-cut adhesion, impact resistance, and gloss retention after acid, alkali water immersion and gel content) that differ in unit, magnitude and direction of merit. A direct comparison is therefore not meaningful, and a formulation that is superior on some criteria but inferior on others cannot be ranked by inspection. A multi-criteria decision-making (MCDM) framework was adopted to resolve this where each criterion was first assigned an objective, data-driven weight, and the weighted criteria were then aggregated into a single overall performance score for each coating. No subjective or expert-assigned weights were used, so the ranking depends only on the measured data.

To ensure that the outcome is not an artefact of a single analytical choice, two conceptually different objective weighting methods, the Shannon entropy method and the CRITIC method were paired with two conceptually different ranking methods, Grey Relational Analysis (GRA) and TOPSIS. Since all four combinations (GRA–entropy, GRA–CRITIC, TOPSIS–entropy and TOPSIS–CRITIC) use the same five-formulation dataset, their agreement shows consistency in the ranking process rather than independent validation. However, agreement across several methods and weighting schemes provides stronger support for the formulation preference than relying on a single approach. All computations were performed in Python.

2.5.1. Decision matrix and normalisation

The problem is expressed as a decision matrix $X = [x_{ij}]$ of $m = 5$ alternatives (coatings, index $i = 1…m$) and $n = 9$ criteria (index $j = 1$-n), where x_{ij} is the value of criterion j for coating i. Every criterion is of the beneficial (“larger-is-better”) type. Two criteria, pencil

ACCEPTED MANUSCRIPT

hardness and cross-cut adhesion, are reported on ordinal grading scales (4H–5H; 3B–5B) rather than continuous measurements. For entry into the decision matrix, the numeral within each grade label was used directly as x_{ij} (e.g., 4H = 4, 5H = 5; 3B = 3, 5B = 5). This assumes that each grade step represents an equal increase in the underlying property. This assumption is common practice when using ordinal test grades in MCDM studies [31], the physical difference between two adjacent grades is not guaranteed to equal the difference between another pair of adjacent grades on the same scale. Direct and indirect impact resistance were treated differently in the multi-criteria framework. Direct impact resistance (inches) is a continuous measurement and was incorporated as the "Impact resistance" MCDM criterion, normalised and weighted in the same manner as the other continuous criteria. Indirect impact resistance, in contrast, was assessed only as pass/fail (EPMCN-1, EPMCN-2 and EPMCN-5 failed; EPMCN-3 and EPMCN-4 passed at 14 in) and was therefore not incorporated as a separate quantitative MCDM criterion, since no non-arbitrary numeric value could be assigned to a "Fail" outcome alongside a continuous pass value. It is instead reported and discussed qualitatively. Notably, EPMCN-3 and EPMCN-4 were the only two formulations to pass indirect impact testing and were also the two top-ranked formulations under every method-weighting combination. This offered independent qualitative support for the ranking despite indirect impact not being a quantitative input to it. Because the criteria are measured in different units, they are normalised before aggregation, and the specific normalisation used (min–max for entropy, GRA and CRITIC; vector normalisation for TOPSIS) is stated with each method.

Accepted Manuscript

ACCEPTED MANUSCRIPT

2.5.2 The Shannon entropy method

The entropy method derives criterion weights from the information content of the data, following the principle from Shannon's information theory that a variable which is more dispersed carries more information [2]. Applied to MCDM, a criterion on which the coatings differ widely is highly discriminating and should carry a large weight, whereas a criterion on which all coatings score almost the same contributes little to the decision and is down-weighted. The method is entirely objective and requires no input beyond the decision matrix, which is why it is one of the most widely used weighting schemes in materials selection.

Each column is first normalised to a probability-like distribution (Eq. 1):

$$p_{ij} = \frac{x_{ij}}{\sum_{i=1}^{m} x_{ij}} \qquad (1)$$

where p_{ij} is the share of criterion j's column total contributed by coating i, so that $\sum_i p_{ij} = 1$. The entropy of each criterion is then (Eq. 2)

$$e_j = -k \sum_{i=1}^{m} p_{ij} \ln p_{ij}, \quad k = \frac{1}{\ln m} \qquad (2)$$

where $e_j \in [0, 1]$ is the Shannon entropy of criterion j and k is a constant that normalises e_j to this range (k = 1/ln 5 = 0.6213 for five coatings); by convention $p_{ij} \ln p_{ij} = 0$ when pij = 0. The physical significance of e_j close to 1 is that the coatings are almost indistinguishable on that criterion (little information can be withdrawn from that criterion), whereas a smaller e_j means the criterion separates them strongly. The information actually provided by the criterion is its degree of divergence (Eqs. 3 and 4),

$$d_j = 1 - e_j \qquad (3)$$

ACCEPTED MANUSCRIPT

$$w_j = \frac{d_j}{\sum_{j=1}^{n} d_j} \quad (4)$$

where d_j is the divergence (information content) of criterion j and w_j is its final entropy weight, normalised so that $\sum_j w_j = 1$. A criterion with identical values for all coatings has $e_j = 1$, $d_j = 0$ and $w_j = 0$, so it cannot influence the ranking, which is the correct mathematical treatment of a non-discriminating property.

2.5.3. Grey Relational Analysis (GRA)

GRA originates in Deng's grey system theory, which was developed for decision problems characterised by a small number of samples and incomplete or "grey" information [19], conditions that apply directly to the present study, with only five formulations. GRA ranks alternatives by their geometric similarity to an ideal reference sequence, and is favoured in materials and coatings research precisely because it is particularly suitable for small-sample decision problems and can be applied without imposing strict distributional assumptions on the data.

The decision matrix is first normalised to the range [0, 1] (grey relational generating). For beneficial criteria (Eq. 5),

$$r_{ij} = \frac{[x_{ij}] - min_i\,[x_{ij}]}{max_i[x_{ij}] - min_i[x_{ij}]} \quad (5)$$

where r_{ij} is the normalised value (a constant criterion is set to 1). The deviation of each coating from the ideal reference sequence $r_{0j} = 1$ (a hypothetical coating that is best on every criterion) is Eq. 6.

$$\Delta_{ij} = |\, r_{0j} - r_{ij} \,| = 1 - r_{ij} \quad (6)$$

where Δ_{ij} is the grey difference; a smaller value means coating i is closer to the ideal on

ACCEPTED MANUSCRIPT

criterion j. These deviations are converted to grey relational coefficients (Eq. 7),

$$\xi_{ij} = \frac{\Delta_{min} + \rho\Delta_{max}}{\Delta_{ij} + \rho\Delta_{max}} \quad (7)$$

where $\xi_{ij} \in (0, 1]$ is the grey relational coefficient (its closeness to the ideal on criterion j); Δ_{min} and Δ_{max} are the global minimum and maximum deviations over the whole matrix (here 0 and 1); and $\rho \in [0, 1]$ is the distinguishing (resolution) coefficient, set to the conventional value $\rho = 0.5$, which balances the influence of near and far deviations. Physical significance: $\xi ij = 1$ when the coating attains the ideal value on a criterion and falls toward 0 as it departs from it. The overall grey relational grade is the weighted average of these coefficients (Eq. 8),

$$\Gamma_i = \sum_{j=1}^{n} w_j \xi_{ij} \quad (8)$$

where Γ_i is the grey relational grade of coating i and w_j are the entropy or CRITIC weights. Γ_i expresses how close, on a weighted average, the coating is to the ideal across all criteria; the coating with the highest Γ_i is ranked first.

2.5.4. CRITIC method

The entropy method judges each criterion in isolation and therefore over-weights information that several criteria share. The CRITIC method (CRiteria Importance Through Intercriteria Correlation) corrects this by combining each criterion's variability with its conflict (statistical independence) relative to the others [3]. It is the appropriate refinement here because several of the mechanical criteria such as hardness, scratch resistance, adhesion and impact which originate from the same underlying network structure and are consequently correlated; CRITIC recognises this redundancy and down-weights such a group rather than counting the same information repeatedly. CRITIC uses

ACCEPTED MANUSCRIPT

the same min–max normalised matrix r_{ij} as GRA (Eq. 5).

The contrast intensity of each criterion is its standard deviation (Eq. 9),

$$\sigma_j = \sqrt{\frac{\sum_{i=1}^{m}(r_{ij}-\bar{r}_j)^2}{m-1}} \tag{9}$$

where σ_j is the standard deviation of the normalised criterion j and $\bar{r}_j$ its mean; σ_j measures how strongly the criterion varies across the coatings. The redundancy between criteria is captured by their linear correlation (Eq. 10),

$$\rho_{jl} = \frac{\sum_{i=1}^{m}(r_{ij}-\bar{r}_j)(r_{il}-\bar{r}_l)}{(m-1)\sigma_j\sigma_l} \tag{10}$$

where ρ_{jl} is the Pearson correlation coefficient between criteria j and l over the m coatings; a value near +1 means the two criteria rank the coatings almost identically and hence carry redundant information. The information content of a criterion combines its variability and its conflict with all others (Eq. 11),

$$C_j = \sigma_j \sum_{l=1}^{n}(1-\rho_{jl}) \tag{11}$$

where C_j is the information content of criterion j. Physical significance: a criterion receives a large C_j only if it is both variable (high σ) and independent of the others (high $\sum(1-\rho)$); a criterion that merely duplicates information already provided by others is penalised even if it is highly variable. The CRITIC weights are Eq. 12.

$$w_j(CRITIC) = \frac{C_j}{\sum_{j=1}^{n} C_j} \tag{12}$$

normalised so that $\sum_j w_j(CRITIC) = 1$. As with entropy, a constant criterion (σ = 0) obtains zero weight. As ρ_{jl} is estimated from only m alternatives, the reliability of individual correlation coefficients and hence the resulting conflict term and CRITIC weights depends on sample size.

Accepted Manuscript

ACCEPTED MANUSCRIPT

2.5.5. TOPSIS

The Technique for Order of Preference by Similarity to Ideal Solution (TOPSIS) ranks alternatives by their simultaneous nearness to a positive-ideal solution and remoteness from a negative-ideal solution [23]. Its underlying principle is that the best compromise choice should be closest to the best-possible and farthest from the worst-possible option; this principle differs fundamentally from the grey-similarity principle of GRA, so applying both provides a genuine cross-check rather than a restatement of the same logic. Following the classical formulation, TOPSIS uses vector normalisation rather than the min–max scaling used above (Eq. 13).

$$n_{ij} = \frac{x_{ij}}{\sqrt{\sum_{i=1}^{m} x_{ij}^2}} \tag{13}$$

where n_{ij} is the vector-normalised value; each raw column is divided by its Euclidean norm, rendering the criteria dimensionless while preserving their proportional differences. The weighted normalised matrix is Eq. 14.

$$v_{ij} = w_j n_{ij} \tag{14}$$

where v_{ij} is the weighted normalised value and w_j is the entropy or CRITIC weight. From $V = [v_{ij}]$ the positive-ideal solution v^+ (the best, i.e. maximum, value of each criterion) and the negative-ideal solution v^- (the worst, i.e. minimum, value) are identified. The separation of each coating from these two reference points is Eq. 15.

$$d_i^+ = \sqrt{\sum_j (v_{ij} - v_j^+)^2} \quad ; \quad d_i^- = \sqrt{\sum_j (v_{ij} - v_j^-)^2} \tag{15}$$

where d_i^+ and d_i^- are the Euclidean distances of coating i from the positive- and negative-ideal solutions. The relative closeness to the ideal is Eq. 16.

ACCEPTED MANUSCRIPT

$$C_i = \frac{d_i^-}{d_i^+ + d_i^-} \quad (16)$$

where $C_i \in [0, 1]$ is the closeness coefficient. Physically $C_i = 1$ identifies a coating that coincides with the ideal solution and $C_i = 0$ one that coincides with the anti-ideal; coatings are ranked in descending order of C_i.

2.5.6 Combined weighting-ranking design

Applying the two weighting schemes (entropy, CRITIC) to the two ranking methods (GRA, TOPSIS) yields four method-weighting combinations, each computed independently in its procedure but applied to the same underlying decision matrix: GRA–entropy, GRA–CRITIC, TOPSIS–entropy and TOPSIS-CRITIC.

2.6 Replicate testing and measurement uncertainty

All the tests, including Pencil hardness, Scratch hardness, Cross-cut adhesion, Impact resistance, Flexibility, Resistance to water, acid, alkali, gel content, swelling studies and solvent rub resistance, gloss measurement and DFT measurements, were performed in triplicate. The pencil hardness and cross cut adhesion tests yielded results having ordinal values. For Flexibility measurement conical mandrel was used which gives numerical values but all the formulations passed the test at minimum diameter (4mm) so it got converted to a binary pass/fail outcome. Scratch hardness and direct impact resistance were determined by a staircase method starting at 2000 g and 15 in, respectively, and decreasing in fixed increments (100 g; 0.5 in) upon failure until the threshold value was identified. Thus, similar triplicate results were obtained which reflect the fixed step resolution rather than an absence of measurement variability.

Gloss (acid, alkali, and water resistance, including the alkali dip degradation of film vs

ACCEPTED MANUSCRIPT

time) and gel content were each measured in triplicate (n = 3). For each property, the sample mean was calculated as Eq. 17.

$$\bar{x} = \frac{1}{n} \sum_{i=1}^{n} x_i \quad (17)$$

where $\bar{x}$ = Mean; n = Total number of data points; x_i = Data point

Sample standard deviation (SD) was calculated as Eq. 18.

$$s = \left[\frac{\sum(x_i - \bar{x})^2}{(n-1)}\right]^{1/2} \quad (18)$$

where s=Sample standard deviation; x_i = Data point; $\bar{x}$ = Mean; n = Total number of data points

Standard error of the mean (SEM) was calculated as Eq. 19.

$$SEM = \frac{s}{n^{1/2}} \quad (19)$$

where s=Sample standard deviation; n= Total number of data points

Expanded Uncertainty was calculated as Eq. 20.

$$U(95\%) = t_{0.975,\,n-1} \times SEM \quad (20)$$

where U= Uncertainty

Measurement uncertainty was expressed as an approximate 95% confidence interval (95% CI), obtained from the standard error of the mean using the Student's t critical value appropriate for n = 3 (t = 4.303 at 2 degrees of freedom), as this better suits the size of the

ACCEPTED MANUSCRIPT

data.

2.7. Gel content

Gel content was determined as per ASTM D2765 with slight modifications. Samples of cured films ($w_{initial}$) with a mass of 30-35 mg were immersed in chloroform (3 mL). This was done for 24 h so as to extract the soluble content. After 24 h, the samples were dried at room temperature until constant weight (w_{final}) was achieved. The gel content of the samples was calculated using Eq. 21 as follows:

$$GC\,(\%) = \frac{W_{final}}{W_{initial}} * 100 \tag{21}$$

These values express percent non-soluble gel content that can be correlated with the crosslink density of the polymers [25, 30].

Swelling was obtained from the same solvent-extraction experiment used for gel content, following the framework of ASTM D2765. The experiment was conducted in triplicate, in which the initial mass before immersion (W_i), the swollen mass immediately on removal from the solvent and before drying (W_s), and the final constant mass after drying (W_f) were measured.

Swelling was calculated as Eq. 22.

$$Swelling\ (\%) = [\frac{(W_s - W_f}{W_f}] \times 100 \tag{22}$$

Both quantities are referenced to the dried, extracted mass W_f because referencing swelling to W_f isolates the behavior of the insoluble network and is independent of how much soluble fraction was removed during extraction [30].

ACCEPTED MANUSCRIPT

2.8. Epoxy Equivalent Weight (EEW) analysis

The epoxy equivalent weight of the samples was evaluated as per IS-9162:1979. The EEW was calculated as follows:

The normality of the HBr solution was calculated using Potassium Hydrogen Phthalate using the formula (Eq. 23).

$$N = A * \frac{1000}{204.2\ B} \tag{23}$$

where A=Amount of Potassium Hydrogen Phthalate used, B=volume of HBr solution used (in mL), The EEW of the resin was calculated as Eq. 24.

$$EEW = \frac{1000*C}{N*(A-B)} \tag{24}$$

where A = Volume of HBr sample used for titration of sample (in mL), B = Volume of HBr sample used for titration of blank (in mL), C = mass of sample used (in grams)

Epoxy Content: Epoxy content can be calculated from EEW by using Eq. 25

$$Epoxy\ Content = \frac{1000}{EEW}\ \text{mmol/g} \tag{25}$$

2.9. Hydroxyl value analysis

The hydroxyl value of the synthesized Phenol Modified Cardanol Novolacs (PMCN) was determined as per ASTM 1957-86 [32]. The hydroxyl value so obtained was reported in mg KOH g^{-1}. It was converted to Hydroxyl group concentration in mmol/g by using Eq 26:

$$OH\ Content\ \left(\frac{mmol}{g}\right) = \frac{OH\ value}{56.1} \tag{26}$$

ACCEPTED MANUSCRIPT

3. Results and Discussion

3.1. Resin characterisation

3.1.1. Epoxy equivalent weight and OH: epoxide ratio

The EEW, phenolic-OH content, epoxide content, and resulting OH:epoxide ratio for each formulation are summarised in Table 1. As phenol content increases, EEW rises and epoxide content falls, since phenol adds no epoxidisable double bond of its own and simply dilutes the cardanol-derived epoxide groups. Phenolic-OH content rises at the same time, since every added phenol unit contributes its own hydroxyl group.

Table 1: Represents the OH: Epoxy ratio in EPMCNs.

S. No.	Sample	EEW	Hydroxyl Value	Phenolic OH content (mmol/g)	Epoxide Content (mmol/g)	OH:Epoxy ratio
1	EPMCN-1/ 0% Phenol	380	127	2.26	2.63	0.86
2	EPMCN-2/ 10% Phenol	410	135	2.41	2.44	0.98
3	EPMCN-3/ 20% Phenol	430	145	2.59	2.33	1.11
4	EPMCN-4/ 30% Phenol	470	157	2.79	2.13	1.31
5	EPMCN-5/ 40% Phenol	520	170	3.03	1.92	1.58

The resulting OH:epoxide ratio rises steadily across the series, from 0.86 at EPMCN-1 to 1.58 at EPMCN-5. This indicates that more hydroxyl groups are available, relative to epoxide groups. As phenolic hydroxyl groups are sterically hindered by the adjacent cardanol side chain, not every -OH group reacts readily during cure; some hydroxyl excess is therefore needed to reliably complete the network despite this hindrance. EPMCN-3 and EPMCN-4 sit in a moderate range on this trend, while EPMCN-5 carries a large excess of phenolic hydroxyls, leaving a correspondingly larger part of unreacted

Accepted Manuscript

ACCEPTED MANUSCRIPT

hydroxyl groups in the cured film.

3.1.2. FTIR

Comprehensive FTIR spectra for this series, together with the full band assignments, are provided in our earlier report [30], which can be referred to for complete spectral detail of both synthetic steps. A new band at 1435 cm^{-1}, absent in cardanol, appears on novolac formation and is assigned to C-H scissoring of the Ar-CH_2-Ar methylene bridges linking adjacent phenolic units. Epoxidation is confirmed by the disappearance of the 3008 cm^{-1} olefinic =C-H stretch together with the simultaneous appearance of three oxirane-ring absorptions (843-847, 1044-1069, and 1233-1241 cm^{-1}), whose combined presence provides more reliable evidence of epoxide formation [30]. This is particularly important because individual bands in this region may overlap with absorptions from other functional groups [30].

3.1.3. ^{1}H NMR

Detailed spectral data, including complete ^{1}H NMR spectra and their integrations, are available in our earlier report [30], to which the reader is requested to refer, for quantitative confirmation. A new Ar-CH_2-Ar methylene-bridge signal at δ 3.88 ppm, absent in the cardanol monomer, intensifies with phenol content (bridge-to-aliphatic integral ratio rising from 0.069 to 0.125, PMCN-1 to PMCN-5), confirming novolac formation. Epoxidation is confirmed by the appearance of oxirane methine/methylene signals (δ 2.70-2.98 and 2.40-2.55 ppm) with a corresponding decrease in the internal olefinic signal (δ 5.34-5.45 ppm), while the terminal vinyl signal is retained throughout,

ACCEPTED MANUSCRIPT

consistent with performic acid's known kinetic preference for internal olefins over terminal.

3.1.4. TGA

The full set of TGA thermograms and the corresponding thermal degradation parameters for all the samples have already been reported in our earlier publication [30], readers seeking the complete dataset can refer to the publication. Dev et.al. show a multistage decomposition, with the main degradation step (250-500 °C) accounting for 62-78% of total mass loss. Both the 5% and 10% mass-loss temperatures rise with phenol content ($T_{5\%}$ rises from 187.5 °C at EPMCN-1 to 237.9 °C at EPMCN-5), and char yield at 800 °C increases correspondingly from 4.15% to 16.59%, consistent with the higher aromatic content contributed by phenol relative to the aliphatic cardanol side chain [30].

3.1.5. DSC Analysis

The complete DSC thermograms for the whole series, along with the extracted thermal transition data, have been documented in our earlier report [30], and readers may refer the publication for the full characterization. Dev et.al. have proposed a self-cure mechanism as no external hardener is present. The cure onset (T_{onset}) falls from 135.8 °C (EPMCN-1) to 117 °C for the phenol-modified resins, consistent with initiation by the resin's own phenolic-OH groups, which open the oxirane ring at a lower temperature than aliphatic OH. The exotherm widens with phenol content, consistent with the two-stage etherification expected for this cure chemistry. Post-cure scans show a flat baseline with no residual exotherm, confirming the cure reaches completion [30].

ACCEPTED MANUSCRIPT

3.2. Gel content and swelling percentage

Gel content and swelling ratio show an inverse relationship. A more extensively converted network retains less soluble material (higher gel content) and absorbs less solvent (lower swelling), while a less-restrictive network shows the opposite pattern. EPMCN-5 shows this most clearly, combining the lowest gel content with the highest swelling. EPMCN-1 and EPMCN-2 show intermediate gel content and correspondingly intermediate swelling. EPMCN-3 and EPMCN-4 show similar values, indicating comparable network formation at these phenol contents. The convergence of these two independently measured properties strengthens confidence in this network-conversion across the series.

Table 2: The gel content and swelling percentage of the EPMCN-1 to EPMCN-5 were [30]:

S.No.	Sample	Gel Content (%)	95% CI	Swelling Content (%)	95% CI
1	EPMCN-1	90.21±0.32	±0.78	260.71±1.41	±3.49
2	EPMCN-2	91.96±3.03	±7.53	243.33±1.89	±4.70
3	EPMCN-3	94.28±2.71	±6.72	233.33±2.80	±6.95
4	EPMCN-4	94.28±2.92	±7.25	236.36±3.75	±9.32
5	EPMCN-5	88.45±0.33	±0.81	312.90±2.82	±6.99

3.3. Film properties

The mechanical and chemical performance of the cured EPMCN films was evaluated to assess the effect of phenol incorporation on coating properties like adhesion, hardness, flexibility, impact resistance and resistance to acid, alkali and water. The results are summarized in Tables 3 to 5.

ACCEPTED MANUSCRIPT

Table 3: Mechanical film properties

Sample	Flexibility	Pencil Hardness	Scratch Hardness (g =grams)	Crosscut Adhesion	Impact (Direct)	Impact (Indirect)	DFT (μm)
EPMCN-1	4 mm	4H	1500	3B	10 in	Fail	30 ±0.2
EPMCN-2	4 mm	4H	1500	3B	12 in	Fail	32±0.2
EPMCN-3	4 mm	5H	2000	5B	14 in	14 in	28±0.2
EPMCN-4	4 mm	5H	2000	5B	14 in	14 in	30±0.2
EPMCN-5	4 mm	4H	1600	4B	8 in	Fail	29±0.2

DFT was controlled to 30±2 μm across all formulations, confirming that the observed property differences are not attributable to variation in coating thickness.

3.3. Mechanical properties

3.3.1. Cross-Cut adhesion

Adhesion to MS substrate improved from 3B (EPMCN-1, EPMCN-2) to 5B (EPMCN-3, EPMCN-4), then declined to 4B (EPMCN-5), as shown in Table 3. The ether linkage formed during curing generates one pendant secondary hydroxyl group [33], which interacts with the oxide layer of mild steel through hydrogen bonding and Lewis-acid base coordination, which is the established adhesion mechanism in epoxy-metal interface [34-36]. As the pendant hydroxyl groups increase as a result of increasing crosslink density the cross-cut adhesion also increases [35]. The loss of adhesion to 4B seen for EPMCN-5 can be attributed to two factors: (i) increased viscosity due to high molecular weight limits the wetting of the substrate during application of the film; and (ii) the unreacted phenolic hydroxyl groups (-OH) self-associate through bulk hydrogen bonding rather than associating with the oxide layer of the substrate [35].

3.3.2. Pencil hardness

Pencil hardness increased from 4H (EPMCN-1, EPMCN-2) to 5H (EPMCN-3, EPMCN-4) and reverted to 4H (EPMCN-5) as shown in Table 3. Pencil hardness shows resistance

ACCEPTED MANUSCRIPT

to slow-rate of plastic deformation and is governed by network stiffness and crosslink density [37, 38]. The change in the pencil hardness from 4H to 5H (4H for EPMCN 1 and EPMCN-2 and 5H for EPMCN 3 and 4) indicates the increase in network conversion due to a better balance in the ratio of phenolic hydroxyl (-OH) to oxirane [37]. The small decline in the pencil hardness of EPMCN-5 can be attributed to lower network conversion [37]. This promotes additional hydrogen bonding among the –OH groups, which is not an alternative to the mechanical contribution of covalent crosslinks but can still provide resistance against slow deformation [39].

3.3.3. Automatic scratch hardness

The scratch hardness of the samples was recorded as 1500 g, 1500 g, 2000 g, 2000 g and 1600 g respectively (from EPMCN-1 to EPMCN-5) as shown in Table 3. Scratch hardness combines elastic recovery with plastic deformation under a dynamic local load and is therefore more sensitive to network connectivity [13]. A network formed by non-covalent associations like hydrogen-bonding sustains its apparent static modulus but cannot effectively dissipate energy during the dynamic local contact of the scratch indenter. This happens because hydrogen bond reorganisation is slower than the contact time of the indenter scratching the surface [40, 41]. The decline in scratch resistance at EPMCN-5 is attributed to an imbalance between phenolic –OH and oxirane groups, which limits crosslink formation and leaves more hydrogen-bonded physical associations within the network [13].

ACCEPTED MANUSCRIPT

3.3.4. Impact resistance

Direct impact resistance rose from 10 in (EPMCN-1) to 14 in (EPMCN-3, EPMCN-4) and dropped to 8 in (EPMCN-5); indirect impact was passed only by EPMCN-3 and EPMCN-4 as shown in Table 3. Impact resistance under high strain-rate loading requires both a dense covalent network (resistance to crack initiation) and sufficient inter-crosslink segmental mobility (energy dissipation without brittle fracture) [42, 14]. EPMCN-1 and 2 fail on modulus owing to their low network formation. EPMCN-3 and EPMCN-4 show an optimized network structure in which high network conversion is balanced by local segmental mobility. The cardanol-derived C_{15} aliphatic chains provide flexible molecular segments around the crosslinking regions, while phenol incorporation modifies the crosslink structure and may increase the effective spacing between successive crosslinking points, thereby helping to reduce excessive brittleness [43, 42, 44]. In EPMCN-5, the high density of phenolic hydroxyl groups introduces extensive inter- and intramolecular hydrogen bonding, which raises the cohesive energy density and acts as physical crosslinks superimposed on the covalent network [45]. Under the rapid loading timescale of the impact test, these hydrogen bonds do not have sufficient time to dissociate and reform [39, 41], effectively restricting segmental mobility and promoting brittle fracture before strain energy can be dissipated [46, 15]. The impact results show brittle failure in EPMCN-5. The directly impacted side survives at 8 in, but the reverse side fails completely. This suggests that the coating has limited ability to absorb and redistribute the impact stress leading to brittle failure on the reverse side.

Accepted Manuscript

ACCEPTED MANUSCRIPT

3.3.5. Flexibility

All five formulations passed the 4 mm conical mandrel test as shown in Table 3. During mandrel bending, the coating deforms slowly, allowing the flexible side chain segment to rearrange and absorb strain [43]. Since the cardanol amount is constant across the series, these flexible segments remain available in comparable amounts. The test results remain constant among the formulations because slow-rate strain permits segmental rearrangement of the inter-crosslink C_{15} segments in every sample, including EPMCN-5 [46, 41]. Although network conversion increases from EPMCN-1 to EPMCN-4, this increases the stiffness of the coatings. However, phenol incorporation also modifies the crosslink network. It increases the spacing between crosslinking points and introduces greater segmental mobility. This added flexibility helps balance the stiffness generated by the higher network conversion [16, 44]. The mandrel results indicate that the side chain of cardanol maintains flexibility across the series. This flexibility is effective under slow bending deformation. Impact response differs because rapid loading gives the network less time for segmental rearrangement and hydrogen-bond re-organisation (Eq. 27) [41, 46].

ACCEPTED MANUSCRIPT

Table 4: Gloss (60°) before/after dip for 36 hours.

Sample	Statistic	Acid Before	Acid After	Alkali Before	Alkali After	Water Before	Water After
EPMCN-1	Mean	89.62	86.90	89.62	40.55	89.62	85.89
	SD	0.60	0.58	0.34	0.34	0.40	0.72
	95% CI	±1.50	±1.45	±0.85	±0.85	±1.00	±1.78
EPMCN-2	Mean	90.94	88.45	90.94	37.17	90.94	88.62
	SD	0.60	0.57	0.36	0.40	0.67	0.44
	95% CI	±1.48	±1.43	±0.89	±1.00	±1.67	±1.10
EPMCN-3	Mean	93.62	91.47	93.62	64.16	93.62	92.61
	SD	0.60	0.58	0.34	0.36	0.40	0.72
	95% CI	±1.50	±1.45	±0.85	±0.89	±1.00	±1.78

ACCEPTED MANUSCRIPT

EPMCN-4	Mean	99.19	97.06	99.19	70.50	99.19	98.27
	SD	0.60	0.57	0.36	0.44	0.67	0.44
	95% CI	±1.48	±1.43	±0.89	±1.10	±1.67	±1.10
EPMCN-5	Mean	92.85	90.27	92.85	35.90	92.85	90.27
	SD	0.60	0.58	0.34	0.34	0.40	0.72
	95% CI	±1.50	±1.45	±0.85	±0.85	±1.00	±1.78

$$Resistance\ is\ gloss\ retention\ (\%) = \frac{mean\ gloss\ after}{mean\ gloss\ before} \times 100 \quad (27)$$

3.3.6. Resistance to water

Water resistance was evaluated by monitoring the change in 60° gloss after immersion as shown in Table 4. The loss in gloss showed a clear dependence on network structure, with the lowest reduction observed near the optimum network-density composition. For EPMCN-1 to EPMCN-5, the changes in 60° gloss values were 3.73, 2.32, 1.01, 0.92, 2.58 units, corresponding to gloss retentions of 95.84, 97.45, 98.92, 99.07, 97.22 %, respectively. Water acts as a hydrogen-bonding plasticiser in epoxy networks, associating with the pendant secondary hydroxyls and unreacted phenolic –OH [47]. This changes the refractive index of the sub-surface layer locally. The two gloss-retention minima sit at opposite compositional extremes (i.e. the minima are seen at EPMCN-1 and EPMCN-5). The reason remains the same: increased water uptake, but via opposite molecular pathways. In EPMCN-1, water uptake is consistent with the greater free volume expected at lower network conversion [48], as can be seen from the lower gel content and higher swelling measured for this formulation. In EPMCN-5, however, excess unreacted phenolic –OH provides hydrogen-bonding sites for water absorption [49]. The optimum at EPMCN-3 and EPMCN-4 combines the highest network conversion due to the best balance between the OH:epoxide ratio, opposite to what is seen in EPMCN-5 which has

Accepted Manuscript

ACCEPTED MANUSCRIPT

excess unreacted hydroxyl [48, 50]. Thus, higher network conversion reduces the free volume and hydrogen-bonding sites available to accumulate water within the film.

3.3.7. Acid resistance

Acid resistance was assessed by measuring the change in 60° gloss after immersion in 5% HCl. Unlike water immersion, the gloss loss remained low and did not show a clear U-shaped dependence on composition. The changes in the gloss values (60°) from EPMCN-1 to EPMCN-5 were 2.72, 2.49, 2.15, 2.13, 2.58 units (96.97–97.85% retention), with the minimum again at EPMCN-3 and EPMCN-4 as shown in Table 4. This indicates the low diffusion coefficient of hydrated H_3O^+ and Cl^- ions into the hydrophobic polymer matrices [51]. The acid interacts with a very thin layer of the coated surface and is not allowed to penetrate deeper into the coating [51]. Within this limited penetration depth, the same factors that control water resistance are still important. The higher network conversion in EPMCN-3 and EPMCN-4 restricts acid-ion entry and reduces gloss change. EPMCN-1 shows greater acid penetration, consistent with the higher free volume expected at its lower network conversion [48, 50]. In EPMCN-5, the higher amount of unreacted phenolic –OH groups increases local polarity and hydrogen-bonding sites [50, 49]. This promotes limited uptake of the acidic aqueous ions and increases gloss loss, even though strong protonation of phenolic –OH is unlikely [52, 53]. The slightly lower gloss loss of EPMCN-1 relative to EPMCN-2, despite its lower network conversion, may be attributed to the higher relative contribution of cardanol-derived C_{15} hydrophobic segments that partially compensate for the lower network density [43]. All the coatings show good acid resistance with EPMCN-3 and EPMCN-4 proving to be slightly better

ACCEPTED MANUSCRIPT

than others.

3.3.8. Alkali resistance and degradation kinetics

After 5% NaOH immersion, EPMCN-1 and EPMCN-5 delaminated completely (adhesion 3B → 0B and 4B → 0B). EPMCN-2 retained only 37.17 % of its gloss (90.94 → 37.17; adhesion 3B → 1B). EPMCN-3 and EPMCN-4 survived as intact films with 64.16% and 70.5% gloss retention respectively (adhesion 5B → 1B and 5B → 2B), with EPMCN-4 emerging as the best alkali-resistant among all the cured films as shown in Table 4 and Figure 1. Alkali attack on phenolic-cured networks is dominated by ionisation of phenolic –OH to phenolate ($Ar–O^- Na^+$), which destroys local hydrophobicity, opens ionic permeation channels, and generates osmotic swelling in the coating [54]. The best alkali resistance requires a dense covalent network and fewer free phenolic –OH groups. EPMCN-4 appears to provide this balance and thus provides the best mechanical and thermal properties. The lower alkali resistance of EPMCN-1 is attributed to easier network swelling and possible alkaline ring opening of unreacted oxirane groups [49]. For EPMCN-5, the higher amount of free phenolic –OH groups can generate phenolate species under alkaline conditions, promoting alkali-assisted degradation despite the higher molecular weight of the resin [49, 50]. The shift of optimum from EPMCN-3 (water and acid) to EPMCN-4 (alkali) identifies strict network conversion as the limiting structural factor under alkaline conditions [50].

Acid and neutral-water exposure left all five coatings essentially unchanged, immersion in 5% NaOH solution produced pronounced and formulation-dependent deterioration, making alkaline attack the decisive chemical challenge for this series. To move beyond a

Accepted Manuscript

ACCEPTED MANUSCRIPT

single end-point rating, the 60° gloss and cross-cut adhesion of each film were monitored over 0, 6, 12, 24 and 36 h of exposure as shown in Table 5 and Figures 1, 2 and 3, allowing the degradation to be treated kinetically.

Table 5: Gloss (60°) after every 6 hours during Alkali Exposure

Sample	Statistic	0 h	6 h	12 h	24 h	36 h
EPMCN-1	Mean	89.62	81.41	73.30	56.87	40.55
	SD	0.34	0.72	0.60	0.57	0.34
	95% CI	±0.85	±1.78	±1.48	±1.43	±0.85
EPMCN-2	Mean	90.94	81.98	73.02	55.09	37.17
	SD	0.36	0.36	0.67	0.44	0.40
	95% CI	±0.89	±0.89	±1.67	±1.10	±1.00
EPMCN-3	Mean	93.62	88.65	83.79	73.96	64.16
	SD	0.34	0.60	0.58	0.34	0.36
	95% CI	±0.85	±1.50	±1.45	±0.85	±0.89
EPMCN-4	Mean	99.19	94.40	89.61	80.13	70.50
	SD	0.36	0.40	0.72	0.60	0.44
	95% CI	±0.89	±1.00	±1.78	±1.48	±1.10
EPMCN-5	Mean	92.85	83.41	73.87	54.89	35.90
	SD	0.34	0.57	0.36	0.67	0.34
	95% CI	±0.85	±1.43	±0.89	±1.67	±0.85

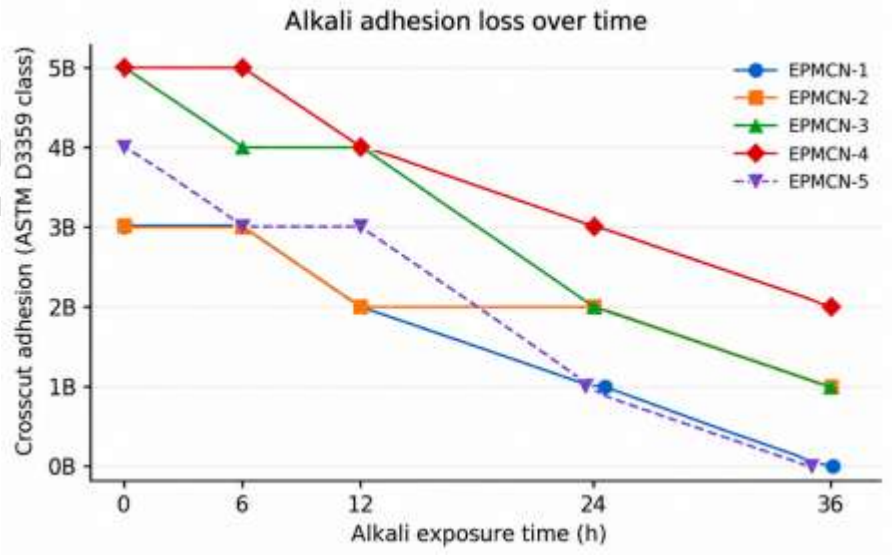


Figure 1: Alkali adhesion loss over time. EPMCN-4 retains the most adhesion; EPMCN-1/5 reach total delamination (0B) by 36 h.

Gloss retention decreased monotonically for every formulation but at strongly divergent

ACCEPTED MANUSCRIPT

rates. The retention–time data conformed closely to first-order behavior, $\ln(G_t/G_0) = -kt$, with coefficients of determination $R^2 \geq 0.975$ for all five coatings as shown in Table 6 and Figure 2, the rate constant k therefore serves as a compact, physically interpretable descriptor of alkali durability. Simple-order kinetic descriptions of this type have precedent in the modelling of gloss loss and property decay in degrading organic coatings [55]. On this basis the series resolves unambiguously into two groups: the near-stoichiometric formulations EPMCN-3 (k = 0.0102 h^{-1}) and EPMCN-4 (k = 0.0092 h^{-1}) degrade slowly, whereas EPMCN-1, EPMCN-2 and EPMCN-5 degrade approximately 2.35 times faster (k = 0.0207–0.0245 h^{-1}) as shown in Table 6 and Figure 3. The corresponding gloss half-lives, t½ = ln2/k, are 68 and 75.3 h for EPMCN-3/4; these values lie beyond the 36 h experimental window and therefore obtained by extrapolation against 28-33.5 h for the remaining films.

Cross-cut adhesion evolved in the same rank order as the gloss values. Alkali resistance is the limiting chemical property of the system, intrinsic to phenolic-cure chemistry, minimised but not eliminated at EPMCN-4. Alkali resistance therefore emerges as the property most sensitive to phenol modification and the clearest kinetic signature of the underlying structure–property relationship in this series (Eq. 28). Gloss retention relative to the 0 h value has been fitted to a first-order model and the parameters are listed in Table 6.

$$retention = 100\, e^{-kt} \qquad (28)$$

Accepted Manuscript

ACCEPTED MANUSCRIPT

Table 6: First-order parameters for alkali-induced gloss loss of the EPMCN coatings.

Sample	Retention at 36h (%)	k (h^{-1})	t½ = ln2/k (h)	R^2
EPMCN-1	45.2	0.0207	33.5	0.983
EPMCN-2	40.9	0.0231	30.0	0.978
EPMCN-3	68.5	0.0102	68.0 *	0.996
EPMCN-4	71.1	0.0092	75.3 *	0.996
EPMCN-5	38.7	0.0245	28.3	0.975

t½ is the time to lose half the initial gloss.

For EPMCN-3/4, gloss retention remained above 50% for the full 36 h exposure window; the t½ values shown are therefore projections from the fitted first-order model beyond the measured range, not directly observed values. The MCDM ranking in Section 3.3 uses the directly measured 36 h retention values, not these extrapolated half-lives, and is therefore unaffected by this limitation.

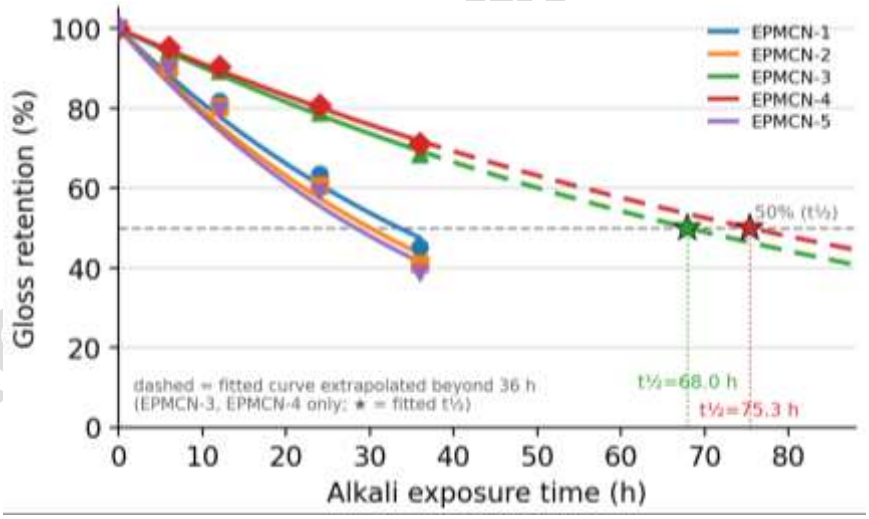


Figure 2: Alkali gloss retention vs exposure time (points) with first-order fits (lines). EPMCN-3/4 retain far more gloss at every time point.

ACCEPTED MANUSCRIPT

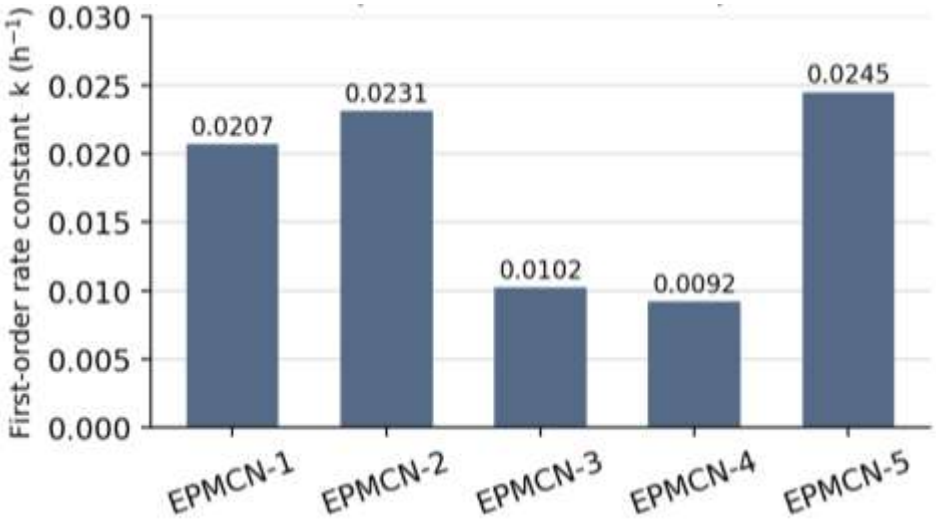


Figure 3: First-order alkali degradation rate constants. EPMCN-3/4 degrade roughly 2.35× slower than EPMCN-1/2/5.

The first-order model provides an excellent empirical description of the alkali-induced gloss loss ($R^2 \geq 0.975$ for all five formulations); given that this fit is based on five experimental time points, it is a well-fitted empirical model.

3.3.9. Solvent resistance

Solvent resistance was assessed by dry film thickness loss after solvent rub testing against xylene, acetone, and methyl ethyl ketone (MEK) as shown in Table 7. To confirm that any difference observed reflects formulation chemistry rather than variation in coating thickness, initial dry film thickness was checked across the panels used for this test and was found to be EPMCN-1: 28.93 ± 0.32 µm; EPMCN-2: 29.29 ± 0.28 µm; EPMCN-3: 29.40 ± 0.27 µm; EPMCN-4: 29.19 ± 0.28 µm; EPMCN-5: 28.52 ± 0.31 µm (Represented as Mean ± SD). All five formulations show the same ordering across all three solvents, with EPMCN-3 and EPMCN-4 losing the least film thickness, followed by EPMCN-2, EPMCN-1, and EPMCN-5. EPMCN-5 lost more thickness than any other

Accepted Manuscript

ACCEPTED MANUSCRIPT

formulation. This pattern is consistent with the network-conversion trend already established by gel content and swelling, and with the mechanical property trends discussed above, reinforcing that solvent resistance tracks the same non-monotonic dependence on phenol content.

Table 7: Solvent resistance of EPMCN coatings: dry film thickness loss (%) after solvent rub testing against xylene, acetone, and MEK

Sample	Solvent	Mean (%)	SD
EPMCN-1	Xylene	4.04	0.89
	Acetone	7.24	0.99
	MEK	10.75	1.53
EPMCN-2	Xylene	2.73	0.67
	Acetone	5.14	1.05
	MEK	7.60	0.95
EPMCN-3	Xylene	0.80	0.53
	Acetone	1.70	0.36
	MEK	3.30	0.74
EPMCN-4	Xylene	1.61	0.53
	Acetone	2.96	0.51
	MEK	4.90	0.80
EPMCN-5	Xylene	6.18	0.91
	Acetone	10.55	1.34
	MEK	15.67	1.80

3.4. Multi-criteria evaluation and ranking:

The property trends favour EPMCN-3/4 but do not yield a single ordering, since the nine criteria differ in scale, direction and importance. A multi-criteria decision-making (MCDM) framework was therefore applied: criteria were weighted objectively by the entropy and CRITIC methods and the coatings ranked by Grey Relational Analysis (GRA) and TOPSIS, giving four independent method–weighting combinations. The decision matrix is given in Tables 3 and 4 and the normalised property profiles in Figure 4. All criteria are beneficial (higher = better).

ACCEPTED MANUSCRIPT

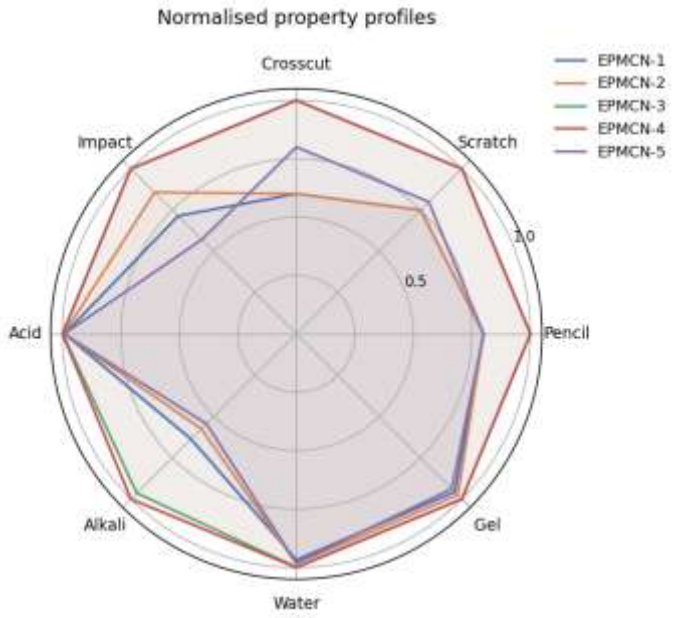


Figure 4. Normalised property profiles (each criterion scaled to its best value; constant flexibility omitted).

3.4.1. Entropy weighting

Each column of the decision matrix was converted to a proportion p_{ij} (Eq. 1; Table 8), from which the Shannon entropy e_j, divergence $d_j = 1 - e_j$ and weight w_j were obtained (Eqs. 2-4; Table 9). A criterion whose values vary little across the coatings has high entropy and hence low weight; the constant flexibility criterion has e = 1 and w = 0. This is the expected outcome for flexibility as the 4 mm mandrel test, is a pass/fail method, and all five formulations passed identically, so flexibility functions here as a screening criterion confirming coating viability rather than a criterion available to discriminate between formulations. Its zero weight under entropy, and the corresponding zero weight obtained under CRITIC (Section 3.3.3), therefore reflect the weighting methods correctly identifying a non-discriminating criterion, rather than an inconsistency in the framework.

ACCEPTED MANUSCRIPT

Table 8. Normalised proportions p_{ij} (Eq. 1).

Sample	Flex	Pencil	Scratch	Crosscut	Impact	Acid	Alkali	Water	Gel
EPMCN-1	0.2000	0.1818	0.1744	0.1500	0.1724	0.1991	0.1711	0.1962	0.1965
EPMCN-2	0.2000	0.1818	0.1744	0.1500	0.2069	0.1997	0.1546	0.1995	0.2003
EPMCN-3	0.2000	0.2273	0.2326	0.2500	0.2414	0.2006	0.2592	0.2025	0.2053
EPMCN-4	0.2000	0.2273	0.2326	0.2500	0.2414	0.2009	0.2688	0.2028	0.2053
EPMCN-5	0.2000	0.1818	0.1860	0.2000	0.1379	0.1996	0.1462	0.1990	0.1926

Table 9. Entropy e_j, divergence d_j and entropy weight w_j (Eq. 2–4).

	Flex	Pencil	Scratch	Crosscut	Impact	Acid	Alkali	Water	Gel
e_j	1.0000	0.9962	0.9944	0.9843	0.9870	1.0000	0.9786	1.0000	0.9998
d_j	0.0000	0.0038	0.0056	0.0157	0.0130	0.0000	0.0214	0.0000	0.0002
w_j	0.0000	0.0636	0.0931	0.2628	0.2180	0.0001	0.3583	0.0008	0.0032

The high entropy weight for alkali resistance results from its large variation among the five formulations, meaning that it statistically distinguishes the formulations more strongly than the other properties. However, the high entropy weight reflects greater variability in alkali resistance across the formulations and should not be interpreted as direct evidence of greater engineering importance [56]. Therefore, statistical importance and practical importance should be considered separately, although they may sometimes agree.

3.4.2 Grey relational analysis

The decision matrix was min–max normalised to r_{ij} (Eq. 5; Table 10). Deviations from the ideal reference sequence, $\Delta_{ij} = |1 - r_{ij}|$ (Eq. 6; Table 11), were converted to grey relational coefficients ξ_{ij} with $\rho = 0.5$ (Eq. 7; Table 12). The weighted sum of ξ_{ij} gives the grey relational grade Γ_i (Eq. 8; Table 13), reported here under both entropy and CRITIC weights.

ACCEPTED MANUSCRIPT

Table 10. Min–max normalised matrix r_{ij} (Eq. 5).

Sample	Flex	Pencil	Scratch	Crosscut	Impact	Acid	Alkali	Water	Gel
EPMCN-1	1.000	0.000	0.000	0.000	0.333	0.000	0.203	0.000	0.302
EPMCN-2	1.000	0.000	0.000	0.000	0.667	0.333	0.068	0.499	0.602
EPMCN-3	1.000	1.000	1.000	1.000	1.000	0.832	0.922	0.953	1.000
EPMCN-4	1.000	1.000	1.000	1.000	1.000	1.000	1.000	1.000	1.000
EPMCN-5	1.000	0.000	0.200	0.500	0.000	0.289	0.000	0.427	0.000

Table 11. Deviation matrix $\Delta_{ij} = |1 - r_{ij}|$ (Eq. 6).

Sample	Flex	Pencil	Scratch	Crosscut	Impact	Acid	Alkali	Water	Gel
EPMCN-1	0.000	1.000	1.000	1.000	0.667	1.000	0.797	1.000	0.698
EPMCN-2	0.000	1.000	1.000	1.000	0.333	0.667	0.932	0.501	0.398
EPMCN-3	0.000	0.000	0.000	0.000	0.000	0.168	0.078	0.047	0.000
EPMCN-4	0.000	0.000	0.000	0.000	0.000	0.000	0.000	0.000	0.000
EPMCN-5	0.000	1.000	0.800	0.500	1.000	0.711	1.000	0.573	1.000

Table 12. Grey relational coefficients ξ_{ij} (Eq. 7, $\rho = 0.5$).

Sample	Flex	Pencil	Scratch	Crosscut	Impact	Acid	Alkali	Water	Gel
EPMCN-1	1.000	0.333	0.333	0.333	0.429	0.333	0.386	0.333	0.417
EPMCN-2	1.000	0.333	0.333	0.333	0.600	0.429	0.349	0.499	0.557
EPMCN-3	1.000	1.000	1.000	1.000	1.000	0.748	0.864	0.915	1.000
EPMCN-4	1.000	1.000	1.000	1.000	1.000	1.000	1.000	1.000	1.000
EPMCN-5	1.000	0.333	0.385	0.500	0.333	0.413	0.333	0.466	0.333

Table 13. Grey relational grades Γ_i and ranks under entropy and CRITIC weights (Eq. 8).

Sample	Γ (entropy)	Rank	Γ (CRITIC)	Rank
EPMCN-1	0.3731	5	0.3679	5
EPMCN-2	0.3980	3	0.4412	3
EPMCN-3	0.9513	2	0.9557	2
EPMCN-4	1.0000	1	1.0000	1
EPMCN-5	0.3820	4	0.3909	4

3.4.3 CRITIC weighting

CRITIC uses the same normalised matrix r_{ij} (Table 14). The standard deviation σ_j of each criterion (Eq. 10; Table 15) measures its contrast, and the Pearson correlation matrix (Eq. 11; Table 16, Figure 5) measures redundancy between criteria. As with the entropy weighting, flexibility's constant value yields $\sigma = 0$ and is therefore excluded from the Pearson correlation matrix, for which correlation is undefined for a constant. The information content $C_j = \sigma_j \Sigma(1 - \rho_{jl})$ and the resulting weight (Eqs. 11-12; Table 16,

ACCEPTED MANUSCRIPT

Figure 6) reward criteria that are both variable and independent. Most mechanical criteria are strongly correlated ($r > 0.9$); CRITIC down-weights them as a group and assigns the largest weight to cross-cut adhesion, followed closely by impact resistance, the two criteria with the lowest correlation to the rest of the set.

As expected when estimating a correlation matrix from a small formulation set, the strength of individual correlation coefficients varies in statistical precision across the matrix. The strongest correlations were observed for pencil-scratch hardness ($\rho = 0.987$) and impact-gel content ($\rho = 0.998$), indicating very strong relationships even with the small sample size. The moderate correlations that most influence CRITIC's differential weighting, such as Impact-Crosscut ($\rho = 0.575$, 95% CI $\approx [-0.62, 0.97]$ by Fisher z-transformation), are estimated with slightly less precision at a given sample size. The reported range provides full statistical transparency and is consistent with standard practice for small-n correlation-based weighting methods. The entropy weighting, does not depend on inter-criteria correlation and provides an independently derived weighting scheme for comparison.

ACCEPTED MANUSCRIPT

Table 14. Standard deviation σ_j of the normalised criteria (Eq. 9).

	Flex	Pencil	Scratch	Crosscut	Impact	Acid	Alkali	Water	Gel
σ_j	0.000	0.548	0.518	0.500	0.435	0.413	0.483	0.413	0.438

Table 15. Pearson correlation matrix ρ_{jl} of the eight varying criteria (Eq. 10).

	Pencil	Scratch	Crosscut	Impact	Acid	Alkali	Water	Gel
Pencil	1.000	0.987	0.913	0.840	0.940	0.987	0.886	0.874
Scratch	0.987	1.000	0.966	0.756	0.947	0.956	0.903	0.797
Crosscut	0.913	0.966	1.000	0.575	0.907	0.854	0.881	0.626
Impact	0.840	0.756	0.575	1.000	0.810	0.856	0.778	0.998
Acid	0.940	0.947	0.907	0.810	1.000	0.893	0.982	0.839
Alkali	0.987	0.956	0.854	0.856	0.893	1.000	0.815	0.887
Water	0.886	0.903	0.881	0.778	0.982	0.815	1.000	0.804
Gel	0.874	0.797	0.626	0.998	0.839	0.887	0.804	1.000

ACCEPTED MANUSCRIPT

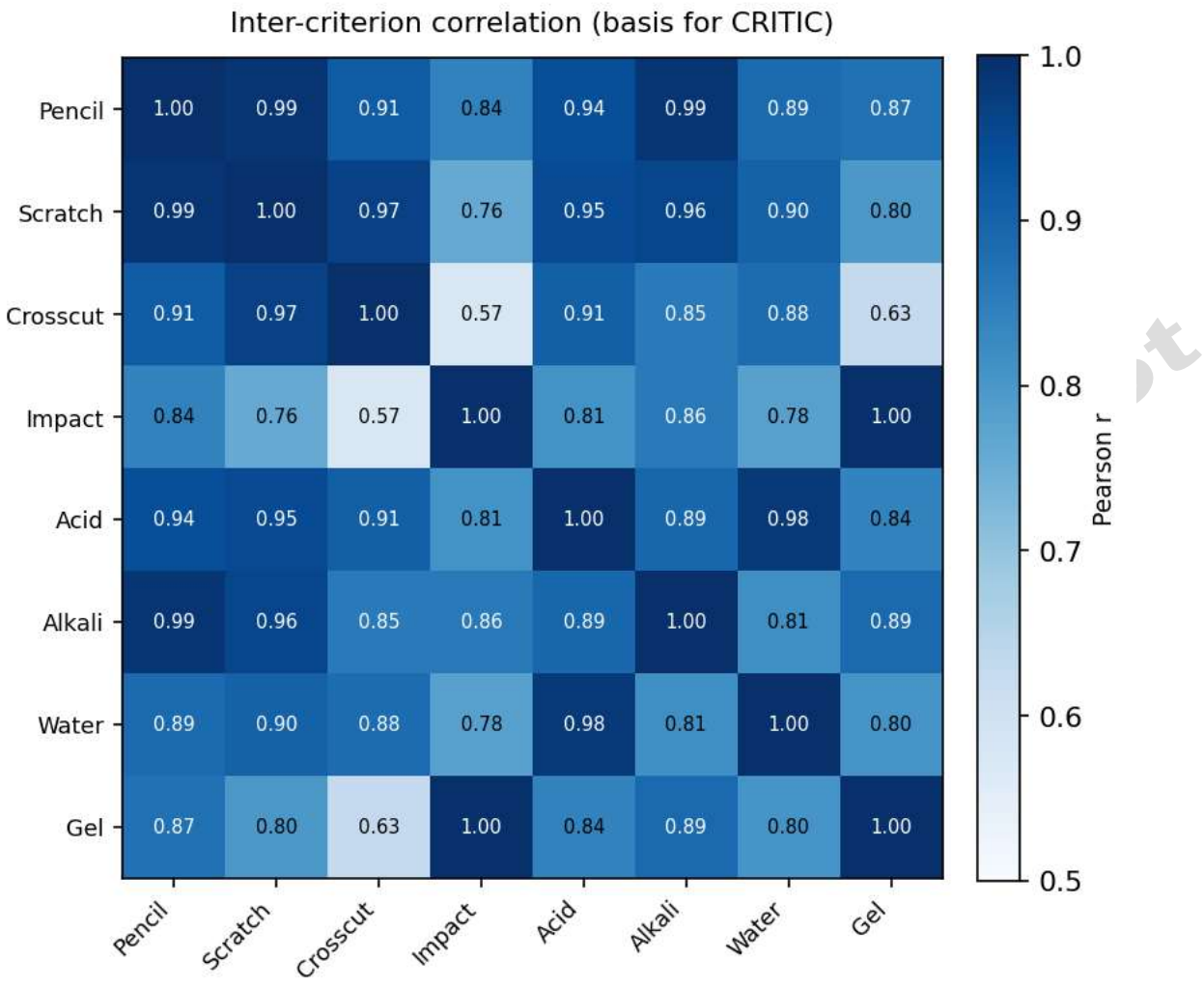


Figure 5. Inter-criterion correlation matrix visualised as a heat map; the pervasive high correlation among the mechanical and gloss criteria is the redundancy that CRITIC corrects for.

Table 16. Conflict $\Sigma(1-\rho)$, information content C_j and CRITIC weight (Eqs. 11–12), with entropy weights for comparison.

Criterion	Conflict	C_j	w_j (CRITIC)	w_j (entropy)
Flexibility	-	0.000	0.0000	0.0000
Pencil hardness	0.573	0.314	0.0906	0.0636
Scratch hardness	0.688	0.356	0.1029	0.0931
Cross-cut adhesion	1.278	0.639	0.1845	0.2628
Impact resistance	1.387	0.603	0.1740	0.2180
Acid gloss retention	0.681	0.281	0.0812	0.0001
Alkali gloss retention	0.752	0.363	0.1048	0.3583
Water gloss retention	0.952	0.393	0.1135	0.0008
Gel content	1.176	0.515	0.1486	0.0032

ACCEPTED MANUSCRIPT

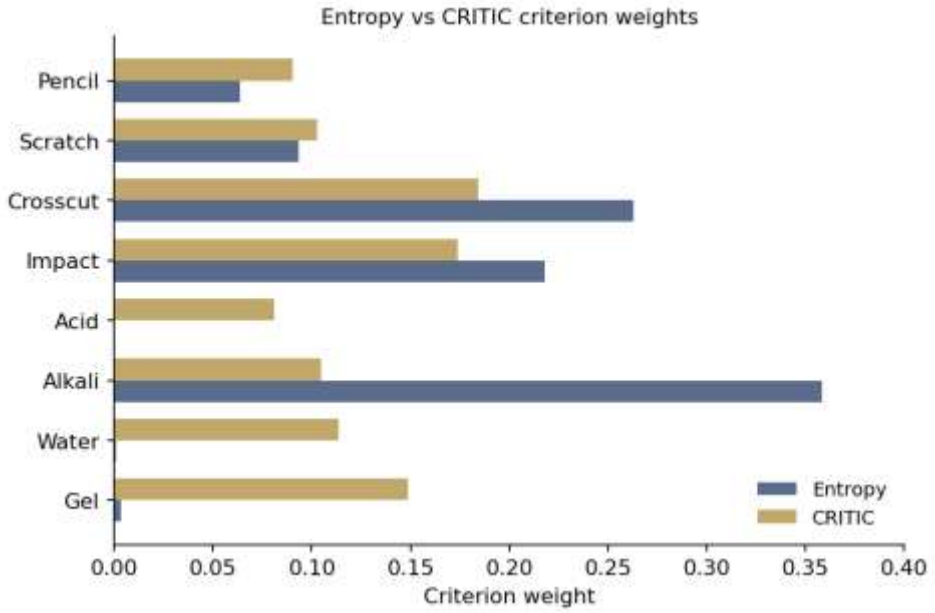


Figure 6. Comparison of entropy and CRITIC criterion weights (flexibility omitted, zero in both).

3.4.4 TOPSIS

TOPSIS used classical vector normalisation, $n_{ij} = x_{ij}/\sqrt{\Sigma x_{ij}^2}$ (Eq. 13; Table 17), followed by weighting, $v_{ij} = w_j n_{ij}$ (Eq. 14; Table 18 shows the entropy-weighted matrix with the positive- and negative-ideal solutions). Euclidean distances to the two ideals (Eq. 15) give the closeness coefficient C_i (Eq. 16; Table 19), reported under both weightings.

Table 17. Vector-normalised matrix n_{ij} (Eq. 13).

Sample	Flex	Pencil	Scratch	Crosscut	Impact	Acid	Alkali	Water	Gel
EPMCN-1	0.447	0.404	0.387	0.327	0.378	0.445	0.370	0.439	0.439
EPMCN-2	0.447	0.404	0.387	0.327	0.454	0.447	0.334	0.446	0.448
EPMCN-3	0.447	0.505	0.515	0.546	0.529	0.449	0.560	0.453	0.459
EPMCN-4	0.447	0.505	0.515	0.546	0.529	0.449	0.581	0.453	0.459
EPMCN-5	0.447	0.404	0.412	0.436	0.302	0.446	0.316	0.445	0.431

Table 18. Weighted normalised matrix v_{ij} (entropy weights) with ideal solutions (Eq. 14).

Sample	Flex	Pencil	Scratch	Crosscut	Impact	Acid	Alkali	Water	Gel
EPMCN-1	0.000	0.0257	0.0360	0.0860	0.0824	0.000	0.1326	0.0003	0.0014
EPMCN-2	0.000	0.0257	0.0360	0.0860	0.0989	0.000	0.1197	0.0003	0.0014
EPMCN-3	0.000	0.0321	0.0480	0.1434	0.1154	0.000	0.2008	0.0004	0.0015
EPMCN-4	0.000	0.0321	0.0480	0.1434	0.1154	0.000	0.2082	0.0004	0.0015
EPMCN-5	0.000	0.0257	0.0384	0.1147	0.0659	0.000	0.1133	0.0003	0.0014

ACCEPTED MANUSCRIPT

v^+	0.000	0.0321	0.0480	0.1434	0.1154	0.000	0.2082	0.0004	0.0015
v^-	0.000	0.0257	0.0360	0.0860	0.0659	0.000	0.1133	0.0003	0.0014

Table 19. TOPSIS distances to the ideals and closeness coefficient C_i under entropy and CRITIC weights (Eqs. 15-16).

Sample	d^+ (ent)	d^- (ent)	C (ent)	Rank	d^+ (CRI)	d^- (CRI)	C (CRI)	Rank
EPMCN-1	0.1014	0.0254	0.2001	5	0.0554	0.0144	0.2058	5
EPMCN-2	0.1076	0.0336	0.2379	3	0.0522	0.0265	0.3367	3
EPMCN-3	0.0075	0.1165	0.9399	2	0.0022	0.0641	0.9671	2
EPMCN-4	0.0000	0.1222	1.0000	1	0.0000	0.0650	1.0000	1
EPMCN-5	0.1114	0.0288	0.2052	4	0.0543	0.0203	0.2723	4

3.4.5. Consolidated ranking

The four combinations are compared in Table 20 and Figures 7 and 8. The ordering EPMCN-4 > EPMCN-3 > EPMCN-2 > EPMCN-5 > EPMCN-1 is now identical across all four method-weighting combinations. The formulations with the weakest overall performance, EPMCN-5 and EPMCN-1, which were previously separated by only hundredths of a unit and interchanged under CRITIC-weighted TOPSIS, now hold a fixed fourth and fifth place in every combination. EPMCN-4 is identified as the best balanced formulation and EPMCN-3 as a close second, the gap to the remaining coatings being governed mainly by alkali durability and network conversion that peaks near the balanced OH:Epoxy stoichiometry of EPMCN-4

Table 20. Ranks (and scores) from all four method–weighting combinations.

Sample	GRA–Ent	GRA–CRI	TOPSIS–Ent	TOPSIS–CRI	Overall
EPMCN-4	1 (1.000)	1 (1.000)	1 (1.000)	1 (1.000)	1
EPMCN-3	2 (0.951)	2 (0.956)	2 (0.940)	2 (0.967)	2
EPMCN-2	3 (0.398)	3 (0.441)	3 (0.238)	3 (0.337)	3
EPMCN-5	4 (0.382)	4 (0.391)	4 (0.205)	4 (0.272)	4
EPMCN-1	5 (0.373)	5 (0.368)	5 (0.200)	5 (0.206)	5

Accepted Manuscript

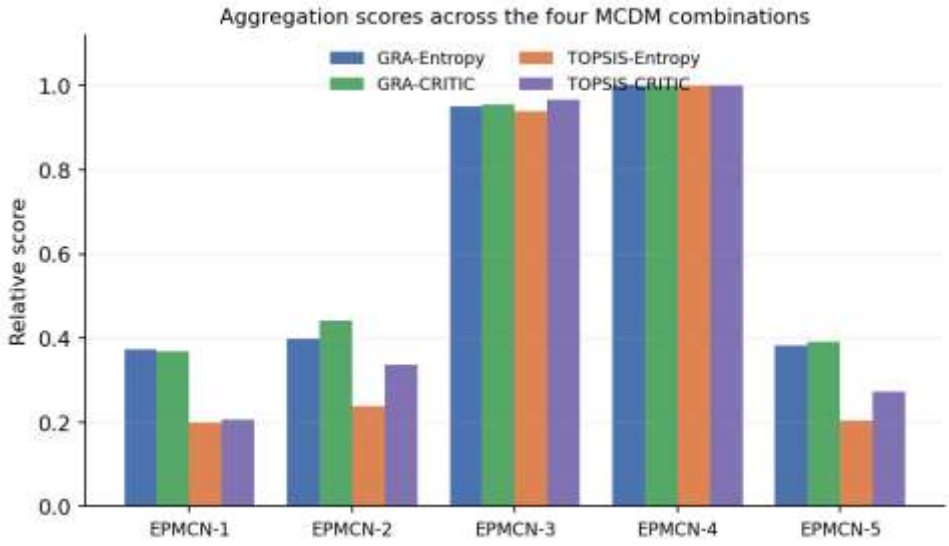


Figure 7. Aggregation scores (grey relational grade Γ and closeness coefficient C) for each coating across the four combinations.

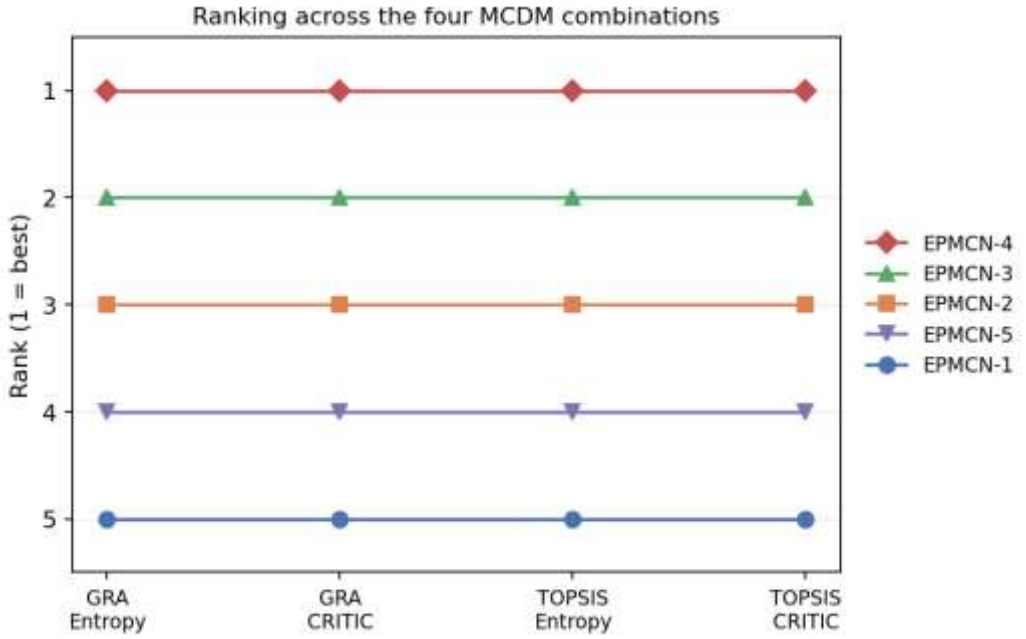


Figure 8. Ranks across the four MCDM combinations; the top three positions are invariant and only EPMCN-5/1 interchange, under CRITIC-weighted.

4. Conclusion

Five self-curable EPMCN coating films were made from 0 to 40% phenol content (molar basis). The resins were characterized using FTIR, ^{1}H NMR, DSC, and TGA. These

ACCEPTED MANUSCRIPT

techniques confirmed novolac formation, epoxidation, and a self-cure mechanism driven by the resin's own phenolic-OH groups. The coatings were then evaluated across nine film properties. Two weighting schemes (Shannon's entropy, CRITIC) and two ranking methods (GRA, TOPSIS) were applied to the dataset. All four combinations gave the same ranking which was EPMCN-4 > EPMCN-3 > EPMCN-2 > EPMCN-5 > EPMCN-1. Alkali exposure was the only test that showed a clear difference between formulations. Acid and water exposure left all films largely unchanged. Alkali-induced gloss loss fit a first-order model well ($R^2 \geq 0.975$). EPMCN-3 and EPMCN-4 degraded about 2.35 times more slowly than the other three formulations. This difference was the largest source of variation among all the properties measured. As a result of this, the entropy and CRITIC weights ranked alkali resistance as the most important criterion. This highlighted alkali resistance as a highly discriminating property among the formulations so, EPMCN-4 was identified as the best-balanced formulation in the series, particularly for uses that need good alkali resistance. EPMCN-3 was ranked second. Solvent resistance against acetone, xylene, and MEK, assessed separately from the ranked criteria, showed the same EPMCN-3/EPMCN-4 advantage, providing independent confirmation of this result.

Future work could examine additional composition variables such as accelerator loading or a finer phenol-content spacing around the observed EPMCN-3/EPMCN-4 optimum, to establish how generally this trend extends beyond the present series. The work could also focus on testing alkali resistance beyond 36-hours. A larger dataset would give more reliable correlation values for the CRITIC method than the five formulations used here.

Accepted Manuscript

Acknowledgements

ACCEPTED MANUSCRIPT

The authors sincerely thank Dr. Pramod Kumar, Visiting Professor, Paint Technology, HBTU Kanpur for their valuable guidance, insightful suggestions, and assistance in the preparation of the manuscript. The authors would also like to thank Mr Shaksham Sonkar PhD. Scholar DOMS HBTU, for his valuable insights.

References

1. Michałowicz J. Bisphenol a – sources, toxicity and biotransformation. Environ Tox Pharm. 2014; 37(2):738-758. https://doi.org/10.1016/j.etap.2014.02.003

2. Caillol S. Cardanol: A promising building block for biobased polymers and additives. Current Opinion Green Sustain Chem. 2018; 14:26-32. https://doi.org/10.1016/j.cogsc.2018.05.002

3. Balachandran VS, Jadhav SR, Vemula PK, John G. Recent advances in cardanol chemistry in a nutshell: from a nut to nanomaterials. Chem Soc Rev. 2013; 42(2):427-438. https://doi.org/10.1039/C2CS35344J

4. Voirin C, Caillol S, Sadavarte NV, Tawade BV, Boutevin B, Wadgaonkar PP. Functionalization of cardanol: towards biobased polymers and additives. Polym Chem 2014; 5(9):3142-3162. https://doi.org/10.1039/C3PY01194A

5. Lubi MC, Thachil ET. Cashew nut shell liquid (CNSL) - a versatile monomer for polymer synthesis. Designed Monom Polym. 2000; 3(2):123–153. https://doi.org/10.1163/156855500300142834

6. Sultania M, Rai JSP, Srivastava D. Studies on the synthesis and curing of epoxidized novolac vinyl ester resin from renewable resource material. European Poly J. 2010; 46(10):2019-2032. https://doi.org/10.1016/j.eurpolymj.2010.07.014

ACCEPTED MANUSCRIPT

7. Yadav R, Awasthi P, Srivastava D. Studies on synthesis of modified epoxidized novolac resin from renewable resource material for application in surface coating. J Appl Poly Sci. 2009; 114(3):1471-1484. https://doi.org/10.1002/app.30581

8. Devi A, Srivastava D. Studies on the blends of cardanol-based epoxidized novolac resin and CTPB. European Poly J. 2007; 43(6):2422–2432. https://doi.org/10.1016/j.eurpolymj.2007.03.006

9. Yadav R, Srivastava D. Blends of cardanol-based epoxidized novolac resin and CTBN for application in surface coating: a study on thermal, mechanical, chemical, and morphological characteristics. J Coat Technol Res. 2010; 7(5):557-568. https://doi.org/10.1007/s11998-009-9235-8

10. Campaner P, D'Amico D, Longo L, Stifani C, Tarzia A. Cardanol-based novolac resins as curing agents of epoxy resins. J Appl Poly Sci. 2009; 114(6):3585-3591. https://doi.org/10.1002/app.30979

11. Hwang C, Yoon K. Multiple attribute decision making: methods and applications a state-of-the-art survey. Berlin Heidelberg: Springer; 1981. https://doi.org/10.1007/978-3-642-48318-9

12. Pirdashti M, Tavana M, Hassim MH, Behzadian M, Karimi IA. A taxonomy and review of the multiple criteria decision-making literature in chemical engineering. IJMCDM. 2011; 1(4):407. https://doi.org/10.1504/IJMCDM.2011.043556

13. Molero G, Sue HJ. Scratch behavior of model epoxy resins with different crosslinking densities. Mater Design. 2019; 182:107965. https://doi.org/10.1016/j.matdes.2019.107965

Accepted Manuscript

ACCEPTED MANUSCRIPT

14. Levita G, De Petris S, Marchetti A, Lazzeri A. Crosslink density and fracture toughness of epoxy resins. J Mater Sci. 1991; 26(9):2348–2352. https://doi.org/10.1007/BF01130180

15. Zheng X, Guo Y, Douglas JF, Xia W. Competing effects of cohesive energy and cross-link density on the segmental dynamics and mechanical properties of cross-linked polymers. Macromolecules. 2022; 55(22):9990-10004. https://doi.org/10.1021/acs.macromol.2c01719

16. Huang J, Fu P, Li W, Xiao L, Chen J, Nie X. Influence of crosslinking density on the mechanical and thermal properties of plant oil-based epoxy resin. RSC Adv. 2022; 12(36):23048-23056. https://doi.org/10.1039/D2RA04206A

17. Achuthamenon Sylajakumari P, Ramakrishnasamy R, Palaniappan G. Taguchi grey relational analysis for multi-response optimization of wear in co-continuous composite. Materials. 2018; 11(9):1743. https://doi.org/10.3390/ma11091743

18. Onyekwere OS, Oladeinde MH, Edokpia RO. Multi-response optimization of bamboo fiber reinforced unsaturated polyester composites using hybrid taguchi – grey relational analysis method. J Indust Prod Eng. 2021; 38(2):98–107. https://doi.org/10.1080/21681015.2020.1848933

19. Chauhan A, Vaish R. Hard coating material selection using multi-criteria decision making. Mater Design (1980-2015). 2013; 44:240–245. https://doi.org/10.1016/j.matdes.2012.08.003

20. Prasad RV, Rajesh R, Thirumalaikumarasamy D. Selection of coating material for magnesium alloy using Fuzzy AHP-TOPSIS. Sādhanā. 2020; 45(1):23. https://doi.org/10.1007/s12046-019-1261-3

ACCEPTED MANUSCRIPT

21. Huang JL, Ding HL, Wang X, Song L, Hu Y. Cardanol-derived anhydride cross-linked epoxy thermosets with intrinsic anti-flammability, toughness and shape memory effect. Chem Eng J. 2022; 450:137906. https://doi.org/10.1016/j.cej.2022.137906

22. Appasamy S, Srinivasan H, Mydeen K M, Kumaravel A, Krishnan A, Muthukaruppan A. Cardanol-phthalein cored benzoxazines for superhydrophobic, corrosion resistant, anti-icing and self-cleaning coatings. European Poly J. 2026; 253:114768. https://doi.org/10.1016/j.eurpolymj.2026.114768

23. Jahan A, Masood S, Zafar F, Rizvi SA, Alam M, Haq QMR, et al. Ambient-cured cardanol-derived polyurea coatings for anti-corrosive and anti-bacterial applications. Prog Org Coat. 2023; 182:107638. https://doi.org/10.1016/j.porgcoat.2023.107638

24. Trivedi R, Raj M, Raj L, Patel R. High-performance fiber-reinforced composites using cardanol-based resin and epoxy resin blend: mechanical, thermal, morphological, and chemical resistance properties with various hardeners. Composite Interf. 2026; 33(6):1349-1373. https://doi.org/10.1080/09276440.2025.2580702

25. Da Silva LRR, Carvalho BA, Pereira RCS, Diogenes OBF, Pereira UC, Da Silva KT, et al. Bio-based one-component epoxy resin: Novel high-performance anticorrosive coating from agro-industrial byproduct. Prog Org Coat. 2022; 167:106861. https://doi.org/10.1016/j.porgcoat.2022.106861

26. Liu Z, Huo J, Yu Y. Water absorption behavior and thermal-mechanical properties of epoxy resins cured with cardanol-based novolac resins and their esterified ramifications. Mater Today Commun. 2017; 10:80-94. https://doi.org/10.1016/j.mtcomm.2017.01.007

Accepted Manuscript

ACCEPTED MANUSCRIPT

27. Athanasopoulos G, Riba CR, Athanasopoulou C. A decision support system for coating selection based on fuzzy logic and multi-criteria decision making. Expert Systems Appl. 2009; 36(8):10848-10853. https://doi.org/10.1016/j.eswa.2009.01.016

28. Kumar S, Maity SR, Patnaik L. Wear parameter optimization of ceramic coating using the fuzzy integrated PSI-CODAS decision-making framework. Arab J Sci Eng. 2023; 48(3):3819-3841. https://doi.org/10.1007/s13369-022-07212-7

29. Shin YJ, Kim M, Hwang SW, Shin MJ, Shin JS. One-component epoxy adhesive for repair of cell phone board. J Adhesion Sci Technol. 2018; 32(12):1278–1286. https://doi.org/10.1080/01694243.2017.1408547

30. Dev Tiwari, Radha Sachan, Arun Maithani, Durgesh Kumar Soni. Structure-property relationship in bio-based epoxy novolacs through phenol modification. Poly Eng Sci. https://doi.org/10.1002/pen.70898

31. Corrente S, Tasiou M. A robust TOPSIS method for decision making problems with hierarchical and non-monotonic criteria. Expert Syst Appl. 2023; 214:119045. https://doi.org/10.1016/j.eswa.2022.119045

32. Mapari S, Mestry S, Mhaske ST. Development of cardanol-derived epoxidized and Si-modified pressure-sensitive adhesives (PSAs). Intern J Adhesio Adhesiv. 2023; 126:103443. https://doi.org/10.1016/j.ijadhadh.2023.103443

33. Parker RE, Isaacs NS. Mechanisms Of epoxide reactions. Chem Rev. 1959; 59(4):737-799. https://doi.org/10.1021/cr50028a006

34. Bahlakeh G, Ghaffari M, Saeb MR, Ramezanzadeh B, De Proft F, Terryn H. A close-up of the effect of iron oxide type on the interfacial interaction between epoxy and carbon

ACCEPTED MANUSCRIPT

steel: combined molecular dynamics simulations and quantum mechanics. J Phys Chem C. 2016; 120(20):11014-11026. https://doi.org/10.1021/acs.jpcc.6b03133

35. Kotb Y, Cagnard A, Houston KR, Khan SA, Hsiao LC, Velev OD. What makes epoxy-phenolic coatings on metals ubiquitous: Surface energetics and molecular adhesion characteristics. J Colloid Interf Sci. 2022; 608:634-643. https://doi.org/10.1016/j.jcis.2021.09.091

36. Semoto T, Tsuji Y, Yoshizawa K. Molecular understanding of the adhesive force between a metal oxide surface and an epoxy resin. J Phys Chem.C. 2011; 115(23):11701-11708. https://doi.org/10.1021/jp202785b

37. Lange J, Luisier A, Hult A. Influence of crosslink density, glass transition temperature and addition of pigment and wax on the scratch resistance of an epoxy coating. J Coat Technol. 1997; 69(9):77-82. https://doi.org/10.1007/BF02696246

38. Yamini S, Young RJ. The mechanical properties of epoxy resins: Part 2 Effect of plastic deformation upon crack propagation. J Mater Sci. 1980; 15(7):1823-1831. https://doi.org/10.1007/BF00550603

39. Bezik CT, Redline EM, Foster JC, Frischknecht AL. Simulations of glass transition and mechanical behavior of off-stoichiometric crosslinked polymers. Macromolecules. 2023; 56(14):5268-5277. https://doi.org/10.1021/acs.macromol.3c00924

40. Rajaee P, Wijesinghe I, Li Z, Yan C. Recent advances in polymeric materials with exceptional mechanical performance achieved *via* multiple hydrogen-bonded networks. RSC Appl Polym. 2025; 3(6):1428-1451. https://doi.org/10.1039/D5LP00189G

Accepted Manuscript

ACCEPTED MANUSCRIPT

41. Cohen N, Du C, Wu ZL. Understanding the dissociation of hydrogen bond based cross-links in hydrogels due to hydration and mechanical forces. Macromolecules. 2021; 54(24):11316-11325. https://doi.org/10.1021/acs.macromol.1c01927

42. LeMay JD, Kelley FN. Structure and ultimate properties of epoxy resins. In: Dušek K, editor. Epoxy Resins and Composites III. Berlin/Heidelberg: Springer-Verlag; 1986. p. 115-148. https://doi.org/10.1007/BFb0035359

43. Kinaci E, Can E, Scala J, Palmese G. Influence of epoxidized cardanol functionality and reactivity on network formation and properties. Polymers. 2020; 12(9):1956. https://doi.org/10.3390/polym12091956

44. Nakka JS, Jansen KMB, Ernst LJ. Effect of chain flexibility in the network structure on the viscoelasticity of epoxy thermosets. J Polym Res. 2011;18(6):1879-1888. https://doi.org/10.1007/s10965-011-9595-5

45. Zheng X, Guo Y, Douglas JF, Xia W. Competing effects of cohesive energy and cross-link density on the segmental dynamics and mechanical properties of cross-linked polymers. Macromolecules. 2022; 55(22):9990–10004. https://doi.org/10.1021/acs.macromol.2c01719

46. Tamrakar S, Ganesh R, Sockalingam S, Haque BZ (Gama), Gillespie JW. Strain rate-dependent large deformation inelastic behavior of an epoxy resin. J Comp Mater. 2020; 54(1):71-87. https://doi.org/10.1177/0021998319859054

47. Zhou J, Lucas JP. Hygrothermal effects of epoxy resin. Part I: the nature of water in epoxy. Polymer. 1999; 40(20):5505-5512. https://doi.org/10.1016/S0032-3861(98)00790-3

ACCEPTED MANUSCRIPT

48. Odegard GM, Bandyopadhyay A. Physical aging of epoxy polymers and their composites. J Polym Sci B Polym Phys. 2011; 49(24):1695-1716. https://doi.org/10.1002/polb.22384

49. Morsch S, Lyon S, Gibbon SR. The degradation mechanism of an epoxy-phenolic can coating. Prog Org Coat. 2017; 102:37-43. https://doi.org/10.1016/j.porgcoat.2016.03.019

50. Morsch S, Lyon S, Greensmith P, Smith SD, Gibbon SR. Water transport in an epoxy–phenolic coating. Prog Org Coat. 2015; 78:293-299. https://doi.org/10.1016/j.porgcoat.2014.08.006

51. Croll SG. Electrolyte transport in polymer barrier coatings: perspectives from other disciplines. Prog Org Coat. 2018; 124:41-48. https://doi.org/10.1016/j.porgcoat.2018.07.027

52. Koeberg-Telder A, Lambrechts HJA, Cerfontain H. Solutes in sulfuric acid. Part VIII. Protonation of phenol, 4-fluorophenol and the 2- and 4-sulfonates of anisole and phenol in concentrated aqueous sulfuric acid; determination of p K_a values by means of ^{13}C NMR. Recl Trav Chim Pays-Bas. 1983; 102(6):293–298. https://doi.org/10.1002/recl.19831020603

53. Lim C, Bashford D, Karplus M. Absolute pKa calculations with continuum dielectric methods. J Phys Chem. 1991; 95(14):5610-5620. https://doi.org/10.1021/j100167a045

54. Flanagin LW, McAdams CL, Hinsberg WD, Sanchez IC, Willson CG. Mechanism of phenolic polymer dissolution: importance of acid-base equilibria. Macromolecules. 1999; 32(16):5337-5343. https://doi.org/10.1021/ma990271y

Accepted Manuscript

ACCEPTED MANUSCRIPT

55. Croll SG. Application and limitations of current understanding to model failure modes in coatings. J Coat Technol Res. 2013; 10(1):15-27. https://doi.org/10.1007/s11998-012-9443-5

56. Kumar R, Singh S, Bilga PS, Jatin, Singh J, Singh S, et al. Revealing the benefits of entropy weights method for multi-objective optimization in machining operations: A critical review. J Mater Res Technol. 2021; 10:1471-1492. https://doi.org/10.1016/j.jmrt.2020.12.114

ACCEPTED MANUSCRIPT